Received: 23 June 2025 | Revised: 3 November 2025 | Accepted: 4 November 2025

DOI: 10.1111/epi.70024

Epilepsia®

RESEARCH ARTICLE

Neuronal hyperexcitability: A key to unraveling hippocampal synaptic dysfunction in Lafora disease

Cinzia Costa[1] | **Laura Bellingacci**[2] | **Jacopo Canonichesi**[3] | **Valentina Imperatore**[3] | **Anna Aurora Taddei**[3] | **Luis Zafra-Puerta**[4,5,6] | **Nerea Iglesias-Cabeza**[4] | **Paolo Prontera**[7] | **Andrea Mancini**[8] | **Massimiliano Di Filippo**[8] | **Alessandro Tozzi**[2] | **Katiuscia Martinello**[9,10] | **Marta Barzasi**[11] | **Fabrizio Gardoni**[11] | **Marina P. Sánchez**[4] | **José M. Serratosa**[4] | **Lucilla Parnetti**[8] | **Miriam Sciaccaluga**[6,12]

[1]Section of Neurophysiopathology S.M. della Misericordia Hospital, Section of Neurology and Laboratory of Experimental Neurology, Department of Medicine and Surgery, University of Perugia, Perugia, Italy

[2]Section of Physiology and Biochemistry, Department of Medicine and Surgery, University of Perugia, Perugia, Italy

[3]Laboratory of Experimental Neurology, Department of Medicine and Surgery, University of Perugia, Perugia, Italy

[4]Laboratory of Neurology, Instituto de Investigación Sanitaria-Fundación Jiménez Díaz, Universidad Autónoma de Madrid (IIS-FJD, UAM), Madrid, Spain

[5]PhD Program in Neuroscience, Universidad Autonòma de Madrid-Cajal Institute, Madrid, Spain

[6]Fondazione Malattie Rare Mauro Baschirotto BIRD Onlus, Longare, Italy

[7]Medical Genetics and Rare Diseases Unit, Maternal-Infantile Department, S.M. Della Misericordia Hospital, Perugia, Italy

[8]Section of Neurology, Department of Medicine and Surgery, University of Perugia, Perugia, Italy

[9]Istituto Neurologico Mediterraneo Pozzilli (Neuromed) - Scientific Institute for Research, Hospitalization and Healthcare (IRCCS), Pozzilli, Italy

[10]Department of Human Sciences Society and Health, University of Cassino and Southern Lazio, Cassino, Italy

[11]Department of Pharmacological and Biomolecular Sciences, University of Milano, Milan, Italy

[12]Department of Life Science, Health, and Health Professions, Link University, Rome, Italy

Correspondence
Cinzia Costa, Section of Neurophysiopathology S.M. della Misericordia Hospital, Section of Neurology and Laboratory of Experimental Neurology, Department of Medicine and Surgery, University of Perugia, Perugia, Italy.
Email: cinzia.costa@unipg.it

Miriam Sciaccaluga, Fondazione Malattie Rare Mauro Baschirotto BIRD Onlus, Longare, Italy and Department of Life Science, Health, and Health Professions, Link University, Rome, Italy.
Email: m.sciaccaluga@unilink.it

Funding information
Associazione Stella Costa di Amalfi; Fondazione Malattie Rare Mauro Baschirotto BIRD Onlus; Spanish

Abstract

Background and Objective: Lafora disease (LD) is a rare progressive disorder caused by mutations in the *EPM2A* or *EPM2B* genes, characterized by the accumulation of Lafora bodies, drug-resistant epilepsy, and cognitive decline. To investigate the early molecular mechanisms of LD, we studied electrophysiological changes in the dentate gyrus (DG) of the *Epm2a*^{R240X} knock-in mouse model at various ages.

Methods: Electrophysiological recordings measured neuronal membrane properties, epileptic-like activity, epileptic thresholds, and synaptic plasticity in *Epm2a*^{R240X} mice at 1, 3, and 12 months. We also employed Periodic Acid–Schiff (PAS) diastase staining, immunofluorescence, and Western blotting to detect Lafora bodies, amyloid beta deposition, and the expression of glutamate receptor subunits.

Results: Epileptic-like activity began at 1 month and intensified with age. Aberrant long-term potentiation (LTP) appeared at 3 months and worsened by

Ministry of Economy, Grant/Award Number: Rti2018-095784b-100SAF MCI/AEI/FEDER; Ministero della Salute, Grant/Award Number: PNRR-MR1-2022-12376430; Centro de Investigación Biomédica en Red de Enfermedades Raras (CIBERER), Grant/Award Number: 23 - U744; Tatiana Pérez de Guzmán el Bueno Foundation; National Institute of Neurological Disorders and Stroke of the National Institutes of Health, Grant/Award Number: P01NS097197; AEVEL Foundation; Italian Ministry of University and Research, Grant/Award Number: 2022CAKAHL and P2022374Y9

12 months. Notably, cannabidiol treatment reduced excitability and restored LTP in older mice, suggesting its potential therapeutic value.

Significance: The reversibility of synaptopathy, even at advanced stages, reinforces the importance of early detection of hyperexcitability and the development of effective therapeutic approaches.

KEYWORDS

cannabidiol, hippocampal synaptic dysfunction, Lafora disease, neuronal hyperexcitability, synaptic plasticity

1 | INTRODUCTION

Lafora disease (LD, OMIM #254780) presents a challenge within the spectrum of rare, progressive neurodegenerative diseases, striking without gender bias.[1] It originates from mutations in the *EPM2A* and *EPM2B* genes,[2–5] which encode laforin and malin, crucial for glycogen metabolism. These mutations lead to the hallmark features of LD, including medication-resistant epilepsy and neurodegeneration,[6] and the accumulation of Lafora bodies (LBs) in cerebral and peripheral tissues.[6,7] The disease typically manifests during adolescence, starting with generalized tonic–clonic seizures, and progressing to cognitive decline, dementia, and increased seizure frequency, ultimately causing complete physical dependency.[6]

Mouse models of LD have been pivotal in deciphering disease mechanisms, particularly the role of LB accumulation in neurodegeneration, and seizure susceptibility.[8–11] These models emphasize the importance of energy metabolism in the brain, connecting impaired glycogenolysis to increased neuronal excitability and lower seizure thresholds.[12] Modified genes in LD mouse models lead to significant neurodegenerative changes, such as autophagy defects, enlarged lysosomes, β deposits, and mitochondrial anomalies.[13] Although patients with LD lack amyloid plaques,[14] age-dependent intraneuronal amyloid beta (Aβ) accumulation has been found in laforin-deficient mice, suggesting a critical role of Aβ accumulation in LD pathology and neuronal aberrant excitability.[13]

The interaction between epilepsy and neurodegeneration is under intense research. Emerging studies suggest that seizures can exacerbate neuronal damage and cognitive decline, emphasizing the need for effective treatments to prevent neurodegenerative outcomes. Aβ accumulation may exacerbate learning disabilities linked to neuronal hyperexcitability.[15,16] In addition, a compelling reciprocal relationship exists between Aβ accumulation and abnormal neuronal excitability, creating a vicious cycle that may contribute to neurodegeneration. These dynamics are supported by both preclinical and clinical studies, indicating that mechanisms driving neurodegeneration in Aβ-related conditions may also play a role in epilepsy, escalating neuronal activity and harming synaptic function and neural network dynamics.[16–18]

Key points

- Epileptiform activity emerges by 1 month in *Epm2a*^{R240X} mice, before Lafora body accumulation.
- Aberrant long-term potentiation (hLTP) appears at 3 months and worsens by 12 months in the dentate gyrus, indicating progressive synaptic dysfunction.
- Cannabidiol restores normal synaptic function in older *Epm2a*^{R240X} mice by reducing hyperexcitability and rescuing physiological LTP.
- Translational relevance: these findings provide a rationale for early-targeted therapies in Lafora disease to prevent or delay progression.

Early abnormalities triggering learning disabilities in LD are not yet understood, highlighting the need for research into the electrophysiological disruptions affecting synaptic communication.[19] Understanding these early pathological mechanisms of LD could unveil potential therapeutic targets and the optimal intervention window.

The *Epm2a*^{R240X} knock-in mouse model, bearing the R240X mutation analogous to the human R241X mutation, exhibits the most severe pathological phenotype among LD models.[11,20] Studies on 12-month-old *Epm2a*^{R240X} mice reveal increased epileptic-like activity and lower pentylenetetrazole (PTZ)-induced seizure thresholds,

alongside aberrant synaptic plasticity in the dentate gyrus (DG). Using this model, we investigated electrophysiological alterations across ages in the DG to unravel the early molecular mechanisms of LD progression. Network hyperexcitability was identified as an early event in LD pathophysiology in this model, preceding the deposition of either LBs or amyloid plaques. Amyloid plaque formation in the DG, may exacerbate LD progression, linked to both neuronal hyperexcitability and synaptic anomalies.

In this scenario, cannabidiol (CBD), which reduces hyperexcitability, holds promise for addressing synaptic plasticity deficits in LD models. CBD is a non-psychoactive *Cannabis sativa* derivative reported to be safe and well tolerated for clinical use.[21,22] Its anti-seizure properties and favorable clinical profile have led to its approval for drug-resistant childhood epilepsy, including Dravet and Lennox–Gastaut syndromes, as well as severe childhood-onset epileptic encephalopathies.[22–24] Our findings show that treating hippocampal slices with CBD reduced hyperexcitability while rescuing synaptic plasticity in the DG of *Epm2a*^{R240X} mice, highlighting the importance of mitigating overexcitability in LD management.

2 | MATERIALS AND METHODS

2.1 | Animals

The *Epm2a*^{R240X} mouse model of LD was generated as reported previously.[8,11] Mice were bred in the Animal Facility Service of the Instituto de Investigación Sanitaria-Fundación Jiménez Díaz, where they were housed in isolated cages in a 12:12 light/dark cycle at constant temperature (23°C), with free access to food and water. Procedures were performed in accordance with the Institutional Animal Care and Use Committee–approved protocol of Cincinnati Children's Hospital and Medical Center. For electrophysiological recordings mice were then transferred to Centro di Ricerca Preclinica of Perugia University and housed in the same conditions described. All procedures involving animals were performed in conformity with the European Directive 2010/63/EU, and following protocols approved by the Animal Care and Use Committee at the University of Perugia (authorization number 08/2018-UT).

2.2 | Periodic Acid-Schiff-diastase staining and immunofluorescence

Periodic Acid–Schiff (PAS)-diastase staining was performed as reported previously.[11] For immunofluorescence, sections were rehydrated in decreasing alcohol concentrations, and antigen retrieval was performed in .1 M sodium citrate buffer (pH 6) at 95°C. Primary antibodies used were anti-nestin (10 μg/mL, R&D Systems, Minneapolis, Minnesota, USA, Cat #AF2736) and anti-Aβ (4G8, 1:250 dilution; Merck, Darmstadt, Germany, Cat. #MABN10). Secondary antibodies were Alexa Fluor 488 (donkey anti-goat, 1:400; ThermoFisher Scientific, Waltham, Massachusetts, USA, Cat. #A32814) and Alexa Fluor 594 (donkey anti-mouse, 1:400; Abcam, Cambridge, UK, Cat. #ab150108). Samples from four to six mice per group were used, with two consecutive sections stained, and evaluated for reproducibility. Images were captured using a Leica DMLB 2 microscope (Leica, Wetzlar, Germany) connected to a Leica DFC320 FireWire digital microscope camera (Leica), and using Zeiss Axioscope 5 (Zeiss, Jena, Germany) connected to an Axiocam 208 color camera (Zeiss). LBs, nestin-positive cells, and Aβ plaques were quantified using ImageJ by two researchers, with values representing the mean of these measurements.

2.3 | Drugs

Bicuculline methiodide, picrotoxin, and CBD were obtained from Tocris Biosciences (Bristol, UK). Drugs were diluted in water (bicuculline), ethanol (picrotoxin), and dimethyl sulfoxide (DMSO;CBD) to 1:1000 for the final solution before experiments. During electrophysiological recordings, solutions were switched to those containing the drugs. The final concentrations of ethanol or DMSO (.1%) did not significantly affect the electrophysiological parameters.

2.4 | Electrophysiology

2.4.1 | Brain slicing

Mice were sacrificed by cervical dislocation. The brain was collected and immersed in ice-cold artificial cerebrospinal fluid (ACSF) containing (in mM): 126 NaCl, 2.5 KCl, 1.2 $MgCl_2$, 1.2 NaH_2PO_4, 2.4 $CaCl_2$, 10 glucose, and 25 $NaHCO_3$, bubbled with 95% O_2 and 5% CO_2, pH 7.4. Transverse hippocampal slices (400 μm for extracellular recordings, 270 μm for patch-clamp) were obtained using a vibratome (Leica, VT 1200S) with iced ACSF. Slices were transferred to a recovery chamber with oxygenated ACSF at 30°C for 30 min, and then at room temperature for 1–2 h before recordings. Each slice was then transferred into the recording chamber and submerged in ACSF at a flow rate of 2.9–3 mL/min at 29°C.

2.4.2 | Patch-clamp recordings

Whole-cell patch-clamp recordings (access resistance 10–15 MΩ; holding potential −70 mV) were performed with a Multiclamp 700B amplifier (Molecular Devices) and borosilicate glass pipettes pulled by a P-97 Puller (Sutter Instruments). Recording pipettes were filled with the K^+-gluconate-based internal solution containing (in mM): 145 K^+-gluconate, .1 $CaCl_2$, 2 $MgCl_2$, .1 ethylene glycol-bis(β-aminoethyl ether)-N,N,N′,N′-tetraacetic acid (EGTA), 10 4-(2-hydroxyethyl)-1-piperazineethanesulfonic acid (HEPES), .3 Na-GTP and 2 Mg-ATP, adjusted to pH 7.3 with KOH. Pipette resistances ranged from 4 to 7 MΩ. Membrane currents were monitored continuously and access resistance, measured in voltage-clamp mode, was in the range of 10–30 MΩ. Membrane capacitance and resistance of DG granule cells were taken online using the membrane seal test function of pClamp 10.7 (−5 mV step, 10 ms). Input resistance (IR) was calculated offline from the slope of the regression line fitted to I–V relationships in the hyperpolarized range (−120 to −110 mV). The inward rectification index (IRI) was computed as the ratio of the absolute current amplitude at −120 mV to the current measured at the resting membrane potential (Vrest) for each recorded neuron. Depolarizing and hyperpolarizing current steps (1200 ms, 50 pA increments) were used for current–voltage curves and action potential (AP) numbers at suprathreshold responses. Depolarizing current steps of increasing amplitudes (5 pA increments) were used to determine the AP threshold. The sag amplitude (Vsag) was defined as the absolute voltage difference between the peak hyperpolarization and the steady-state potential during a −120 mV current step, whereas the sag ratio was calculated as (Vpeak − Vss)/Vpeak, thus normalizing sag to the maximal deflection. AP amplitude and rise time were quantified from the first suprathreshold AP evoked by minimal current injection, with amplitude defined as the difference between resting potential and peak; and rise time as the interval from 10% to 90% of the upstroke. Fast afterhyperpolarization (fAHP) amplitude was measured from threshold to the negative peak following the AP, and fAHP duration was taken as the time from AP threshold to return to baseline. Phase–plane plots (dV/dt vs V) were constructed from the first AP obtained with the incremental step protocol used to determine the AP threshold, in order to analyze spike initiation and repolarization dynamics. For spontaneous excitatory postsynaptic currents (sEPSCs), picrotoxin (50 μM) was added to ACSF to block γ-aminobutyric acid A ($GABA_A$) currents, with neurons clamped at −70 mV. Data were acquired with pClamp 10.7 (Molecular Devices), filtered at .1 kHz, digitized at 200 μs using Clampex 10.7, analyzed offline with automatic detection, and manually verified for accuracy.

2.4.3 | Extracellular recordings

The stimulating electrode was inserted into perforant path fibers and the recording electrode, made of borosilicate glass capillaries filled with 2 M NaCl (resistance 10–15 MΩ), it was placed in the DG close to the granular layer. Stimuli of .1 Hz, 10 ms duration, and 20–30 V amplitude evoked field excitatory post-synaptic potentials (fEPSPs) that in the DG included a population spike (PS) that was 50% of maximum amplitude. The PS amplitude was defined as the average of the amplitude from the peak of the early positivity to the peak negativity and of the amplitude from the peak negativity to the peak late positivity. Axoclamp 2B amplifier (Molecular Devices) was used. Traces were filtered at 3 kHz, digitized at 10 kHz, and stored in a PC. To induce long-term potentiation (LTP) in the DG hippocampal region, a high-frequency stimulation (HFS) protocol, consisting of three trains of 1 s (5 min intervals) was delivered at 100 Hz[11] after acquiring a stable baseline for 10 min.

2.4.4 | Epileptic-like activity and epileptic threshold

Epileptic-like activity in hippocampal DG was induced by perfusing slices with an Mg^{2+}-free external solution, in the presence of bicuculline.[11] The epileptic-like activity was measured both as the mean number of the PSs and as PS amplitude %, as reported previously.[11] A time course of the amplitude of the PSs in percentage is thus obtained. A similar protocol, removing bicuculline from the solution, can be used to assess epileptic threshold.

2.5 | Western blotting

Tissues were homogenized at 4°C in ice-cold buffer containing .32 M sucrose, .1 mM phenylmethylulfonyl fluoride (PMSF), 1 mM HEPES, 1 mM MgCl, and 1 mM NaF, protease inhibitors (Complete, Sigma-Aldrich), and phosphatase inhibitors (PhosSTOP, Sigma-Aldrich). Protein samples were separated by Sodium Dodecyl Sulfate–PolyAcrylamide Gel Electrophoresis (SDS-PAGE) and transferred to nitrocellulose membranes. Membranes were blocked for 1 h at room temperature (I-block, TBS 1X, 20% Tween 20), and then incubated overnight at 4°C with primary antibodies: rabbit anti-GluA1 (WB 1:1000, #13185S, Cell Signaling), mouse anti-GluA2 (WB 1:2000, #75-002, Neuromab), mouse anti-GluA3 (WB 1:1000, #MAB5416, Millipore), rabbit anti-phosphoSer845-GluA1 (WB 1:1000, #ab76321, Abcam), rabbit anti-GluN2A (WB 1:1000, #M264, Sigma-Aldrich), rabbit anti-GluN2B (WB

1:1000, #14544s, Cell Signaling), rabbit anti-ERK (WB 1:1000, #9102, Cell Signaling), rabbit anti-phosphoERK (WB 1:1000, #9101, Cell Signaling), and mouse anti-tubulin (WB 1:10000, #T9026, Sigma-Aldrich). After washes, membranes were incubated with secondary antibodies (goat anti-rabbit HRP, #1706515; goat anti-mouse HRP, #1706516, Bio-Rad) for 1 h at room temperature, developed using ECL reagents (Bio-Rad) and scanned with a Chemidoc (Bio-Rad) using Image Lab software. Protein bands were quantified as relative optical density (OD), normalized to tubulin, and expressed as a percentage of the control mean.

2.6 | Statistical analysis

Data analysis was performed using Clampfit 10.7 (Molecular Devices) and GraphPad Prism 9.0 (GraphPad Software, Inc.). Values are expressed as mean ± SEM. The "*n*" indicates the number of cells or field potentials recorded for electrophysiological analysis and the number of animals for histology. For statistical analysis we used two-way analysis of variance (ANOVA), Student's *t* test, or the Mann–Whitney test, with significance set at $*p < .05$. No differences in basal membrane properties, epileptic-like activity, or synaptic plasticity were found between young (1–3 months) and old (6–12 months) wild-type (WT) mice (data not shown), so data from these groups were pooled for analysis.

3 | RESULTS

3.1 | Age-dependent alterations of neuronal membrane properties in the DG of *Epm2a*^{R240X} mice

To investigate changes in the intrinsic electrical membrane properties in DG granule cells of *Epm2a*^{R240X} mice, patch-clamp recordings were performed in hippocampal slices from 1-, 3-, and 12-month-old *Epm2a*^{R240X} mice and age-matched WT animals. DG cells from *Epm2a*^{R240X} animals presented increased membrane resistance at resting potential, lower membrane capacitance, and a reduced time constant as early as 3 months (Figure 1A). Current–voltage relationship analysis and resting membrane potentials (V_{rest}) revealed significant age-dependent differences, with reduced inward currents at hyperpolarizing voltage steps, and a hyperpolarized V_{rest} in *Epm2a*^{R240X} animals as early as 3 months compared to WT (Figure 1B). To shed light on potential alterations in conductances at hyperpolarized potentials, we measured input resistance (Rin) and the IRI from the I-V plots. Analysis of Rin between −120 and −110 mV revealed a significant increase in *Epm2a*^{R240X} DG cells at 12 months, compared to WT (Figure 1C left panel). IRI, calculated as the ratio of the current amplitude at −120 mV to that at the resting potential, revealed a progressive age-dependent reduction in *Epm2a*^{R240X} cells (Figure 1C). In particular, at 1 month, IRI values were comparable to WT, but by 3 months they were significantly reduced, and by 12 months, inward rectification was nearly abolished, indicating a progressive loss of inward rectifier currents with age in *Epm2a*^{R240X} granule cells. In order to further assess the contribution of hyperpolarization-activated currents, we quantified the amplitude of Vsag and sag ratio during hyperpolarizing steps (Figure 1D). At 1 month, *Epm2a*^{R240X} neurons displayed Vsag and sag ratio values similar to WT. However, a significant decrease in Vsag and Sag ratio was observed at 12 months of age in *Epm2a*^{R240X} cells compared to WT, consistent with reduced activation of sag current (Figure 1D).

To assess possible changes in intrinsic excitability, we analyzed AP properties using a current clamp step protocol. The number of APs evoked was similar in *Epm2a*^{R240X} and WT cells except at the first depolarizing current step. Specifically, in 12-month-old *Epm2a*^{R240X} mice, a 50 pA current injection elicited significantly more APs compared to WT (Figure 2A). In line with this, rheobase current was significantly reduced in these cells (Figure 2B), an effect likely linked to the more hyperpolarized AP threshold observed at 12 months in the *Epm2a*^{R240X} neurons (Figure 2B). To better assess AP properties, we compared AP amplitude, rise time, and fAHP between WT and *Epm2a*^{R240X} cells at 1, 3, and 12 months of age (Figure S1). AP peak amplitude was comparable between WT and *Epm2a*^{R240X} at 1 and 3 months but was significantly reduced in *Epm2a*^{R240X} neurons at 12 months compared with age-matched controls (Figure S1A). In contrast, AP rise time and fAHP remained unchanged across groups and ages (Figure S1B–D). Alterations in the dynamics of AP initiation and repolarization may not be fully captured by conventional waveform parameters, and to address this, we performed an AP phase–plane analysis, which provides a sensitive readout of Na^+ and K^+ conductance dynamics during spike generation. Phase–plane analysis confirmed the lower AP threshold in mutant cells compared to WT at different ages and revealed moderate changes in both activation and repolarization slopes. These findings suggest altered activity or expression of key conductances, including Nav1.6 and voltage-gated K^+ channels such as Kv4.2, SK, and Kv7 (Figure 2C).

Analysis of the sEPSCs in DG granule cells revealed no differences between WT and *Epm2a*^{R240X} animals (Figure S2).

3.2 | Epileptic-like activity and aberrant LTP in 3-month-old *Epm2a*^{R240X} mice

Because 12-month-old *Epm2a*^{R240X} mice have been reported to display aberrant excitability of DG

granule cells and epileptic-like activity, we aimed to explore earlier time points in this model to identify precocious events in LD progression.

Epileptic-like activity was induced in hippocampal slices of 1-, 3-, and 12-month-old *Epm2a*^{R240X} mice and age-matched controls. The PS number and amplitude were significantly increased in all ages of *Epm2a*^{R240X} mice compared to WT animals, in an age-dependent manner, indicating more intense epileptic-like activity in 12-month-old *Epm2a*^{R240X} mice relative to younger mice (Figure 3A). Of interest, epileptic-like activity was comparable between 1- and 3-month-old *Epm2a*^{R240X} mice, suggesting that network hyperexcitability is a very early event in the progression of this pathology, potentially preceding LBs deposition (Figure S3) in this model.

To better dissect age-dependent differences, epileptic threshold parameters were analyzed in 1- and 3-month-old *Epm2a*^{R240X} mice (see Methods section), measuring PS number and amplitude. We previously reported a lower epileptic threshold in 12-month-old *Epm2a*^{R240X} mice compared to WT.[11] No significant differences were found between young *Epm2a*^{R240X} and WT mice (Figure 3B), indicating that the lower epileptic threshold is displayed only by older *Epm2a*^{R240X} mice. Taken together, these data suggest that the DG of *Epm2a*^{R240X} mice may exhibit altered network excitability as early as 1 month, although less than in older mice.

Because Aβ peptides are involved in neuronal hyperexcitability linked to synaptic and network dysfunction in various neurodegenerative models,[16] we hypothesized that amyloid plaque formation in the DG might play a

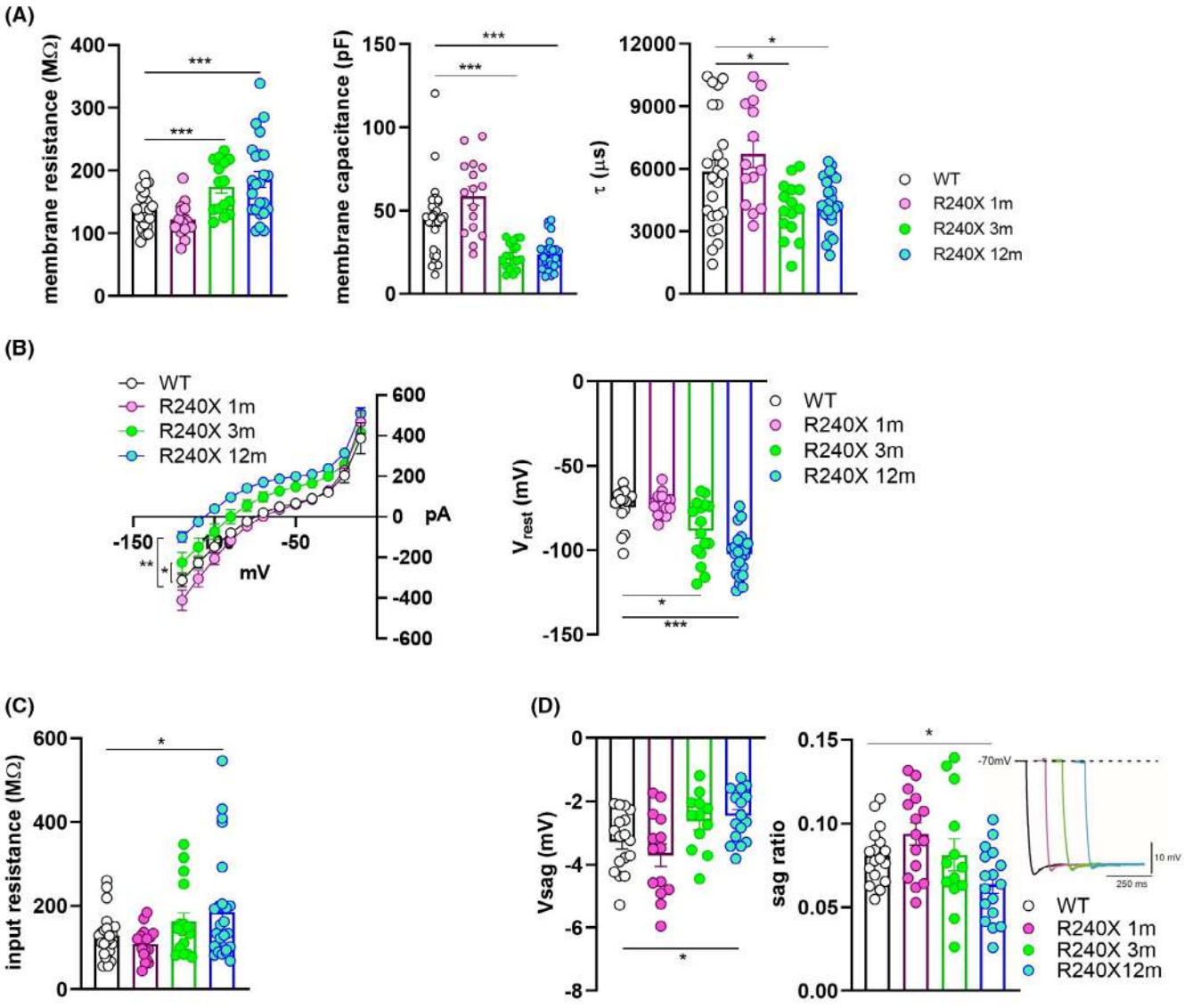

FIGURE 1 Intrinsic membrane properties of DG granule cells in 1-, 3- and 12-month-old *Epm2a*^{R240X} mice. (A) Bar charts showing significative age-dependent increase of membrane resistance (Rm) and reduction of membrane capacitance (Cm) and time constant (τ) (Rm: WT = 136.9 ± 5.37 MΩ, n = 27; 1m-R240X = 122.2 ± 7.54 MΩ, n = 14, p = .124 vs WT; 3m-R240X = 174.6 ± 10.5 MΩ, n = 15, p = .001 vs WT; 12m-R240X = 185.6 ± 12.7 MΩ, n = 24, p = .0006 vs WT; Cm: WT = 44.9 ± 4.33 pF, n = 27; 1m-R240X = 58.8 ± 5.53 pF, n = 16, p = .057 vs WT; 3m-R240X = 22.9 ± 1.85 pF, n = 18, p = .0003 vs WT; 12m-R240X = 23.67 ± 1.83 pF, n = 27, p = .0001 vs WT; τ: WT: 5847 ± 571 µs, n = 24; 1m-R240X: 6708 ± 656 µs, n = 14, p = .33 vs WT; 3m-R240X: 4067 ± 346 µs, n = 15, p = .0115 vs WT; 12m-R240X: 4413 ± 254 µs, n = 24, p = .0284 vs WT; unpaired Student's t test with Welch's correction). (B) Mean current–voltage plot showing significant age-dependent alterations in *Epm2a*^{R240X} mice (WT: n = 25; 1m-R240X: n = 10, p = .475, $F_{(1,39)}$ = .52 vs WT; 3m-R240X: n = 17, p = .03, $F_{(1,40)}$ = 5.06 vs WT; 12m-R240X: n = 27, p < .0001, $F_{(1,50)}$=53.21 vs WT; two-way ANOVA). Right: Bar graph highlighting the age-dependent hyperpolarization of the resting membrane potential in *Epm2a*^{R240X} mice (WT: −74.56 ± 3.04 mV, n = 15; 1m-R240X: −72.87 ± 1.75 mV, n = 15, p = .63 vs WT; 3m-R240X: −88.44 ± 4.45 mV, n = 16, p = .016 vs WT; 12m-R240X: −102.5 ± 2.61 mV, n = 24, p < .0001 vs WT; unpaired Student's t test with Welch's correction). (C) Bar graphs showing input resistance (left) and inward rectifying index (I_{-120mV}/I_{Vrest}) (right) measured from dentate granule cells of WT (black), 1- (magenta), 3- (green), and 12-month-old (blue) *Epm2a*^{R240X} mice. Input resistance displayed an upward trend, reaching statistical significance at 12 months (WT = 128.3 ± 11.2 MΩ, n = 23; 1m-R240X = 108.0 ± 9.7 MΩ, n = 16, p = .18 vs WT; 3m-R240X = 162.0 ± 20.5 MΩ, n = 17, p = .16 vs WT; 12m-R240X = 185.2 ± 24.9 MΩ, n = 26, p = .004 vs WT; unpaired Student's t test with Welch's correction). Inward rectifying index was significantly reduced in *Epm2a*^{R240X} at 3 and 12 months of age (WT = 64.14 ± 14.2, n = 24; 1m-R240X = 75.76 ± 22.4, n = 16, p = .66 vs WT; 3m-R240X = 22.26 ± 6.3, n = 17, p = .011 vs WT; 12m-R240X = 11.66 ± 2.6, n = 26, p = .0013 vs WT; unpaired Student's t test with Welch's correction), indicating an age-dependent alteration in inward rectification. (D) Bar graphs and representative traces showing sag potential (left) and sag ratio (right). Left: Absolute sag amplitude (Vsag, mV) showed a trend toward reduction in *Epm2a*^{R240X} neurons, reaching statistical significance at 12 months compared with WT (WT = −3.28 ± .2 mV, n = 17; 1m-R240X: −3.71 ± .3 mV, n = 15, p = .32 vs WT; 3m-R240X: −2.63 ± .3 mV, n = 13, p = .077 vs WT; 12m-R240X: −2.46 ± .2 mV, n = 17, p = .012 vs WT; unpaired Student's t test with Welch's correction). Right: Sag ratio displayed a significant reduction in 12-month old *Epm2a*^{R240X} mice (WT: .08 ± .004, n = 17; 1m-R240X: .094 ± .007, n = 15, p = .11, vs WT; 3m-R240X: .081 ± .01, n = 13, p = .97 vs WT; 12m-R240X: .063 ± .005, n = 17, p = .013 vs WT; unpaired Student's t test with Welch's correction). Data are presented as mean ± SEM; circles in bar graphs represent individual cells. *p < .05, **p < .01, ***p < .001.

role in LD pathophysiology. A progressive significant increase in 4G8-positive deposits was found in the DG of 12-month-old *Epm2a*^{R240X} compared to WT mice (Figure 4A–C).

We therefore investigated the LTP of DG granule cells. We previously reported abnormally increased LTP in the DG of 12-month-old *Epm2a*^{R240X} mice compared to WT mice.[11] This aberrant LTP is likely due to neuronal hyperexcitability (hLTP) and is associated with cognitive and learning impairments.[11] *Epm2a*^{R240X} mice at 3 months also displayed increased LTP compared to WT (Figure 4C). Comparing 3- and 12-month-old knock-in mice revealed a significant reduction in LTP amplitude at 3 months. Of interest, LTP in the DG of 1-month-old *Epm2a*^{R240X} mice is preserved at physiological levels. These results, suggest that hyperexcitability precedes both synaptic deficits and LBs and Aβ deposition in this LD model.

Given the role of ionotropic receptors in synaptic plasticity, the expression levels of α-amino-3-hydroxy-5-methyl-4-isoxazolepropionic acid (AMPA) and *N*-methyl-D-aspartate (NMDA) receptor subunits were analyzed in total homogenates prepared from hippocampal DG areas. As shown in Figure S4A and B, western blot analysis revealed no alteration in the protein levels of the GluN2A and GluN2B subunits of NMDA receptors or the GluA1, GluA2, and GluA3 subunits of AMPA receptors in *Epm2a*^{R240X} compared to WT mice. In addition, evaluation of phosphorylation levels (pThr845) of the GluA1 subunit, relevant for receptor anchoring at the postsynaptic membrane,[25] and phosphorylation of the signaling protein ERK (pERK/ERK) showed no significant change (Figure S4C).

We then investigated whether the lower epileptic threshold and aberrant LTP could result from increased hippocampal neurogenesis.[26] To this end, nestin-expressing progenitor cells[27] were labeled in the hippocampus of WT and *Epm2a*^{R240X} mice at 3 and 12 months of age (Figure S5A). Quantification revealed that *Epm2a*^{R240X} mice exhibit more progenitor cells in all hippocampal regions compared to WT mice at 12 months, but not at 3 months (Figure S5B–G).

3.3 | Modulating neuronal hyperexcitability rescues LTP in the DG of 12-month-old *Epm2a*^{R240X} mice

We then assessed whether reducing hyperexcitability with CBD could counteract aberrant synaptic plasticity in this LD model at 12 months. The optimal concentration of CBD was established by a dose–response curve of its effects on synaptic transmission. After a stable PS response for 10 min, CBD was bath applied for 20 min at 1–30 µM. CBD dose-dependently reduced PS amplitude compared to baseline, with a maximum effect at 30 µM (Figure 5A).

The highest CBD dose that did not affect physiological transmission (3 μM) was tested for its ability to rescue electrophysiological alterations and epileptic-like activity in the DG of 12-month-old *Epm2a*^{R240X} mice. CBD restored the current–voltage relationship (Figure 5B), the resting membrane potential, as well as the input resistance and the inward rectifying index of *Epm2a*^{R240X} mice granule cells to control levels (Figure 5C). CBD also reduced the number of action potentials in *Epm2a*^{R240X} animals (Figure 5D) by normalizing the rheobase current and the threshold potential (Figure 5E) and restored both Vsag and sag ratio to control levels (Figure 5F). Phase–plane

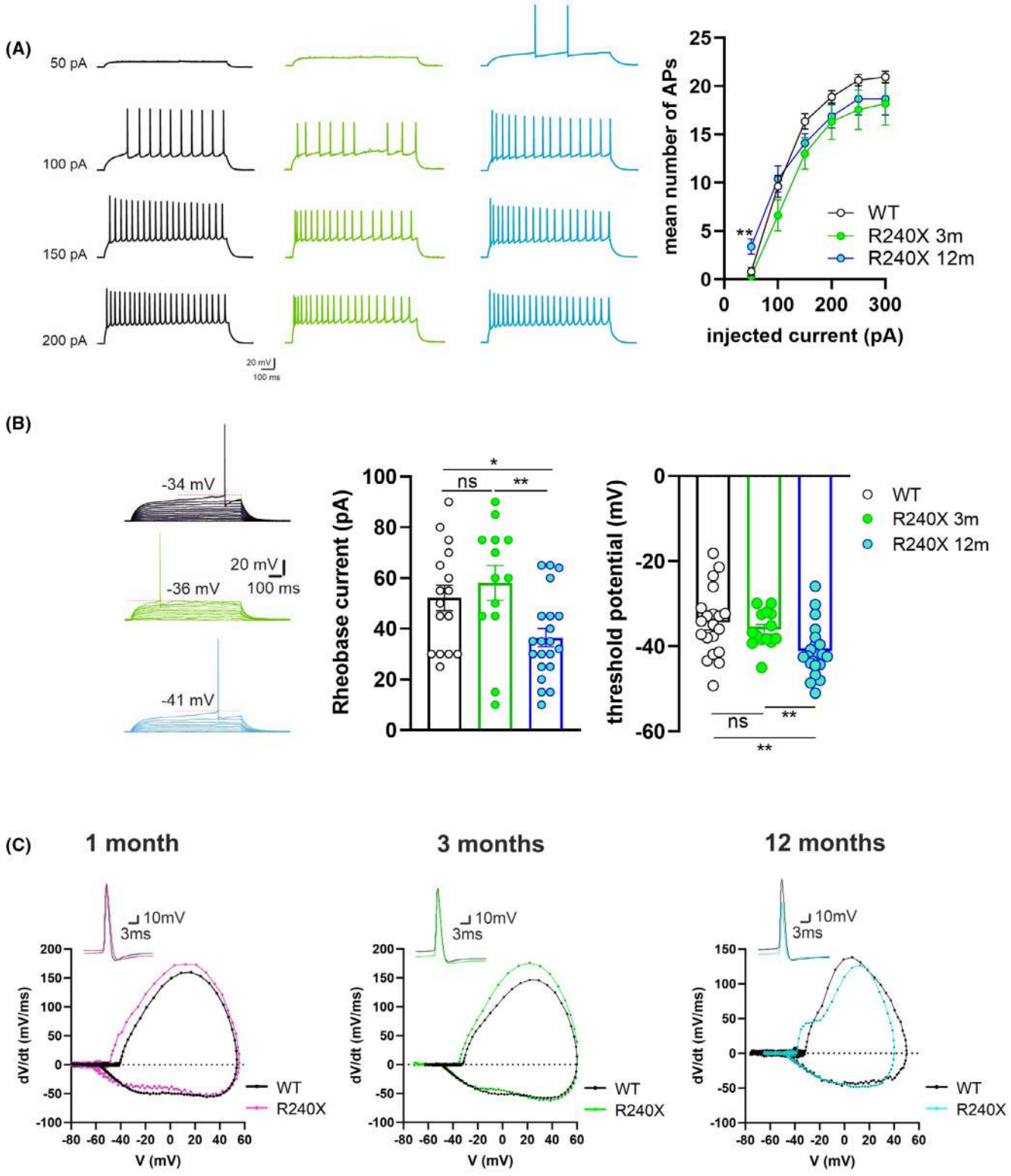

FIGURE 2 Time-dependent alterations in intrinsic excitability and action potential dynamics of dentate granule cells in R240X mice. (A) Patterns of action potential (AP) firing in WT (black) and *Epm2a*^{R240X} mice at 3 (green) and 12 (cyan) months. The plot representing the mean number of AP shows a significant difference in the firing pattern discharge elicited by the first step of depolarizing current injected between WT and 12-month-old *Epm2a*^{R240X} mice (WT: .61 ± .4, $n = 15$; 3m-R240X: .3 ± .1, $n = 13$, $p = .27$ vs WT; 12m-R240X: 1.9 ± .8, $n = 10$, $p = .0088$ vs WT; unpaired Student's t test with Welch's correction). (B) Current–clamp recordings (5 pA–stepped depolarizing current injections; 1 s), scaled to show AP threshold (red dotted line), in WT (black) and *Epm2a*^{R240X} mice at 3 (green) and 12 (cyan) months. Bar graphs showing a significant reduction of the rheobase current (middle, WT: 52.19 ± 5.04 pA, $n = 16$; 3m-R240X: 58.08 ± 6.8 pA, $n = 13$, $p = .48$ vs WT; 12m-R240X: 36.48 ± 3.6 pA; $n = 21$, $p = .013$ vs WT; $p = .0045$ 3m-R240X vs 12m-R240X; unpaired Student's t test with Welch's correction) and a hyperpolarized threshold potential (right, WT: −34.4 ± 1.76 mV, $n = 20$; 3m-R240X: −36.02 ± 1.14 mV, $n = 14$, $p = .49$ vs WT; 12m-R240X: −41.16 ± 1.33 mV; $n = 21$, $p = .0037$ vs WT; $p = .0098$ 3m-R240X vs 12m-R240X; unpaired Student's t test with Welch's correction) in 12-month-old *Epm2a*^{R240X}. Values are reported as mean ± SEM; circles in bar graphs represent individual cells. *$p < .05$, **$p < .01$. (C) Phase–plane analysis of action potentials in dentate granule cells from WT and R240X mice at different ages. Representative phase–plane plots (dV/dt vs membrane potential) are shown for neurons recorded at 1 month (left, WT in black, *Epm2a*^{R240X} in magenta), 3 months (middle, WT in black, *Epm2a*^{R240X} in green), and 12 months (right, WT in black, *Epm2a*^{R240X} in blue). Insets illustrate representative single action potential waveforms recorded in current-clamp configuration under each condition (calibration: 10 mV, 3 ms).

analysis after CBD application resulted in a steeper rising phase with respect to *Epm2a*^{R240X} and a phase–plane trajectory that largely overlapped with WT (Figure 5G).

Moreover, CBD completely restored epileptic-like activity, both with and without bicuculline (Figure 6A,B), and rescued the aberrant LTP to control levels in the DG of *Epm2a*^{R240X} mice (Figure 6C). These data demonstrate that enhanced excitability of DG granule cells underlies aberrant synaptic plasticity and that counteracting hyperexcitability may be a valuable strategy to rescue LTP.

4 | DISCUSSION

This study demonstrates that network hyperexcitability is an early event in the pathophysiology of LD, occurring before the deposition of LBs and Aβ, and prior to synaptic deterioration (Figure 7). Furthermore, our research highlights progressive changes in synaptic plasticity within the DG of the *Epm2a*^{R240X} model, marked by early alterations in neuronal excitability, a pattern observed in models of other neurodegenerative disorders, such as Alzheimer's disease.[28,29] These findings suggest that intervention with targeted treatments during the early stages of the disease, potentially before the onset of neurological clinical symptoms in humans, could significantly influence disease progression. Therefore, identifying and capitalizing on this early therapeutic window is crucial for effectively modifying the disease course. Of note, previous studies have demonstrated that neuronal dysfunction in LD is not restricted to the DG but also affects other brain regions, including the frontal cortex, basal ganglia, and cerebellum,[30,31] highlighting the widespread nature of circuit alterations and further supporting the need for early and system-level therapeutic strategies.

The mechanisms underlying aberrant excitability and synaptic dysfunction in LD remain unknown. Neurodegeneration and seizure susceptibility in LD have been correlated with LB deposition.[10] However, recent evidence demonstrates abnormalities in dendritic spines and cognitive-behavioral deficits in LD mouse models long before LBs appear,[19] suggesting early alterations in synaptic communication that may underlie neuronal excitability, leading to epileptogenic events and cognitive impairment. The complex bidirectional relationship between epilepsy and cognitive decline remains a matter of scientific debate. Clinical and preclinical evidence suggests that they are closely intertwined[15,18] and may share common pathophysiological mechanisms[16,17] that need further elucidation. Thus, it is possible to hypothesize that hyperexcitability is the *primum movens* of cognitive decline in LD.

Our previous work demonstrated enhanced excitability and lower epileptic threshold, along with aberrant hyperplasticity (hLTP) in the DG of 12-month-old *Epm2a*^{R240X} mice, whereas the CA1 region remained unaffected.[11] This aligns with previous studies showing that increased excitability drives enhanced synaptic transmission and LTP magnitude in the DG,[29,33] and that this dysfunction spreads spatiotemporally, from the DG to the CA1.[33] Thus, hyperexcitability and neurodegeneration appear as a continuum encompassing epilepsy and cognitive decline, with aberrant excitatory activity triggering compensatory mechanisms that lead to a loss of homeostatic plasticity, contributing to network dysfunction in a self-powering loop.[15,16] In this scenario, the aberrant LTP observed in the DG of older *Epm2a*^{R240X} mice seems to be based on hyperexcitability and can be defined as hLTP.[11]

To understand the early mechanisms of the disease, we investigated whether alterations in the DG of 12-month-old *Epm2a*^{R240X} mice were present in younger (1- and 3-month-old) mice. We first examined the intrinsic membrane properties of DG granule cells in WT and *Epm2a*^{R240X} mice across different ages. At 1 month, most passive properties, including resting membrane potential

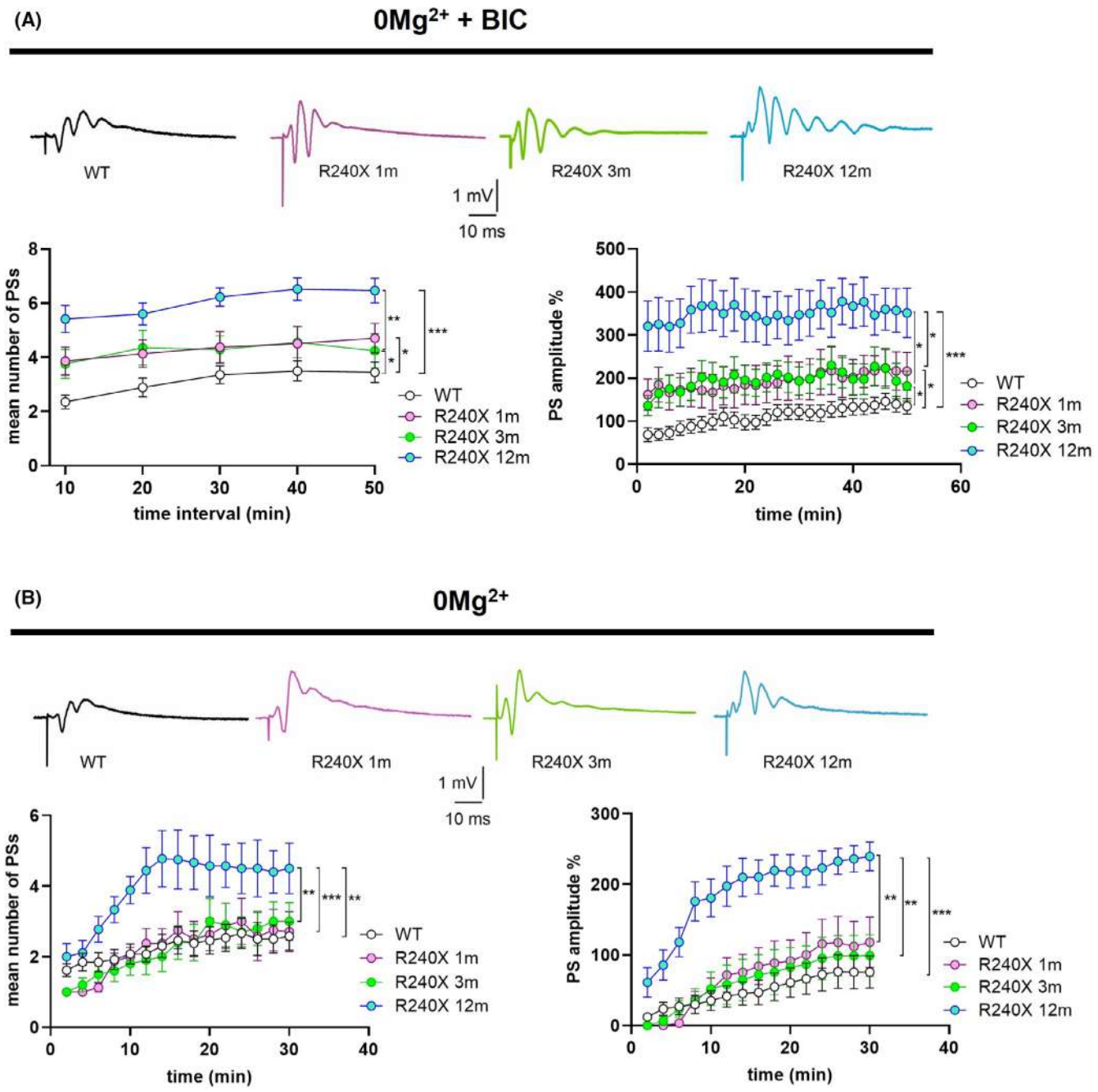

FIGURE 3 Epileptic–like activity in DG slices of 1-, 3- and 12-month-old *Epm2a*^{R240X} mice. (A) Representative traces of FPs (upper panel) and time-course graph (lower panels) of the mean number (left) and amplitude (right) of PSs recorded in the DG of WT (black), 1- (pink), 3- (green), and 12-month-old (cyan) *Epm2a*^{R240X} mice in a magnesium-free ACSF in the presence of .1 μM bicuculline, showing a time-dependent increase of the epileptic-like activity in LD mice (*PS number*: WT: 3.4 ± .4, $n = 21$; 1m-R240X: 4.7 ± .5, $n = 8$, $p = .03$, $F_{(1,27)} = 5.2$ vs WT; 3m-R240X: 4.2 ± .6, $n = 10$, $p = .042$, $F_{(1,28)} = 4.53$ vs WT; 12m-R240X: 6.5 ± .4, $n = 14$, $p < .0001$ $F_{(1,31)} = 52.54$ vs WT; *PS amplitude*: WT: 135 ± 17.9%, $n = 26$; 1m-R240X: 216 ± 34.8%, $n = 10$, $p = .046$, $F_{(1,34)} = 4.29$ vs WT; 3m-R240X: 182 ± 34.8%, $n = 10$, $p = .024$, $F_{(1,35)} = 5.54$ vs WT; 12m-R240X: 351 ± 57.0%, $n = 18$, $p < .0001$, $F_{(1,916)} = 659$ vs WT; $p = .037$, $F_{(1,21)} = 4.96$ 1m-R240X vs 12m-R240X; $p = .025$, $F_{(1,22)} = 5.81$ 3m-R240X vs 12m-R240X; two-way ANOVA). (B) Representative traces of field potentials (FPs) (upper panel) and time-course graph (lower panels) of the mean number (left) and amplitude (right) of PS measured in the DG of WT (black) and *Epm2a*^{R240X} mice at 1 (pink), 3 (green), and 12 (cyan) months of age, in a magnesium-free ACSF in the absence of bicuculline, showing the lower epileptic threshold in 12-month-old *Epm2a*^{R240X} mice (PS number: WT: 2.6 ± .4, $n = 13$; 1m-R240X: 2.7 ± .6, $n = 7$, $p = .89$ vs WT; 3m-R240X: 3.0 ± .53, $n = 8$, $p = .83$ vs WT; 12m-R240X: 4.5 ± .72, $n = 6$, $p = .0012$ vs WT; $p < .0001$ 1m-R240X vs 12m-R240X; $p = .0014$ 3m-R240X vs 12m-R240X; *PS amplitude*: WT: 75.8 ± 22.9%, $n = 10$; 1m-R240X: 118 ± 35.8%, $n = 8$, $p = .30$ vs WT; 3m-R240X: 99.1 ± 29.5%, $n = 10$, $p = .46$ vs WT; 12m-R240X: 240 ± 20.3%, $n = 11$, $p < .0001$ vs WT; $p = .0029$ 1m-R240X vs 12m-R240X; $p = .0015$ 3 m-R240X vs 12m-R240X; two-way ANOVA). Data are reported as means ± SEM, *n* refers to the number of slices.

and input resistance, were comparable between groups, but subtle alterations were already detectable. In particular, the time constant (tau) was reduced in *Epm2a*^{R240X} neurons, suggesting an increased responsiveness to ionic currents, a parameter considered a sensitive predictor of hyperexcitability.[34] At 3 months, age-dependent differences became more evident. Current–voltage relationships revealed reduced inward current amplitudes at hyperpolarized potentials and a significant reduction of the IRI. Since inward rectification is mediated mainly by Kir and HCN channels,[35–37] the progressive loss of IRI suggests impaired function of these conductances.

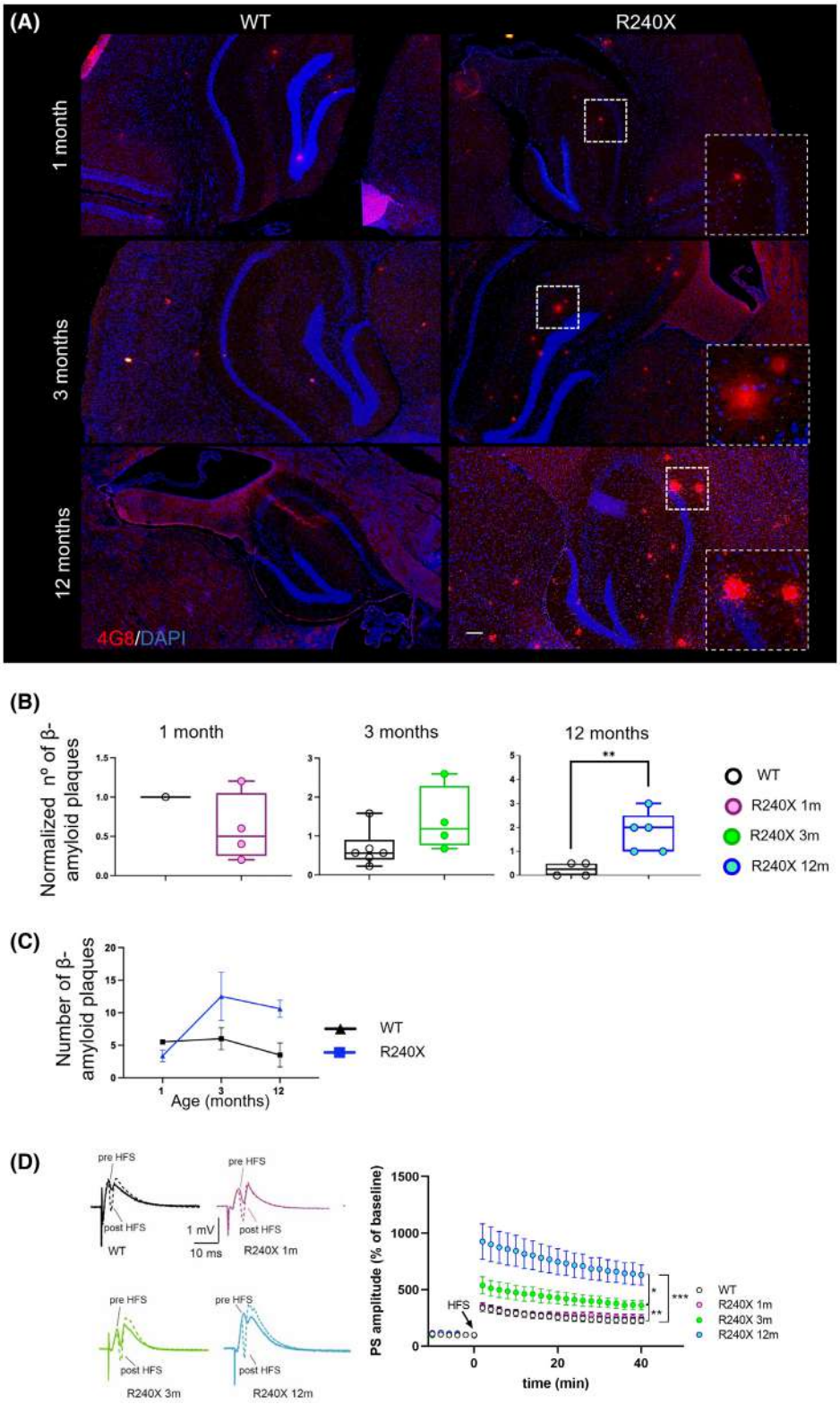

FIGURE 4 Quantification of amyloid beta (Aβ) plaques and time-dependent LTP alteration in the DG of WT and *Epm2a*^{R240X} mice. (A) Immunofluorescence using the 4G8 antibody revealed abundant presence of Aβ plaques in the hippocampal region of WT and *Epm2a*^{R240X} mice. (B) Quantitative comparison of amyloid deposits in the hippocampus at 1, 3, and 12 months of age (1 month old: WT vs *Epm2a*^{R240X} $p = .4684$; 3 months old: WT vs *Epm2a*^{R240X} $p = .0857$; 12 months old: WT vs *Epm2a*^{R240X} $p = .0397$). (C) Aβ depositions with age in the hippocampus of WT and *Epm2a*^{R240X} mice (WT 1 month old vs 3 months old: $p = > .9999$; WT 1 month old vs 12 months old: $p = .9982$; WT 3 months old vs 12 months old: $p = .9427$; *Epm2a*^{R240X} 1 month old vs 3 months old: $p = .0731$; *Epm2a*^{R240X} 1 month old vs 12 months old: $p = .1789$; *Epm2a*^{R240X} 3 months old vs 12 months old: $p = .9848$). Data are shown as the median of independent samples. Whiskers in box plots indicate the minimum and maximum values. For statistical analysis, a non-parametric Mann–Whitney test and two-way ANOVA with Tukey's multiple comparisons test were carried out. Scale Bar = 100 μm. $n = 1$–6 mice per genotype. (D) Representative PS traces recorded before (continuous line) and 40 min after (dotted line) the HFS protocol in DG slices of WT (black), 1- (pink), 3- (green), and 12-month-old (cyan) *Epm2a*^{R240X} mice. The time–course plot of PS amplitudes recorded in the DG before and after HFS protocol shows a time-dependent hyper-plasticity in LD mice. Note that 1-month-old *Epm2a*^{R240X} mice display a physiological LTP (WT: 230 ± 26.4%, $n = 13$; 1m-R240X: 250 ± 31.4%, $n = 5$, $p = .68$, $F_{(1,16)} = .18$ vs WT; 3m-R240X: 437 ± 52.4%, $n = 9$, $p = .006$, $F_{(1,19)} = 9.56$ vs WT; 12m-R240X: 632 ± 89.3%, $n = 9$, $p = .0001$, $F_{(1,20)} = 22.74$ vs WT; $p = .0137$, $F_{(1,12)} = 8.34$ 1m-R240X vs 12m-R240X; $p = .032$, $F_{(1,15)} = 5.35$, 3m-R240X vs 12 m-R240X; two-way ANOVA). Data are reported as means ± SEM, *n* refers to the number of slices. *$p < .05$, **$p < .01$, ***$p < .001$.

Kir dysfunction weakens the cell's ability to stabilize the potential near EK,[38] whereas impaired HCN activity reduces the depolarizing sag that normally opposes hyperpolarization and contributes to temporal integration.[39–41] Functionally, this results in reduced subthreshold stability and increased excitability, consistent with the observed changes in Rin and tau.

At 12 months, excitability was overtly enhanced in *Epm2a*^{R240X} neurons. These cells displayed reduced rheobase current, hyperpolarized threshold potential, and an increased number of action potentials elicited by the first depolarizing current step. These findings suggest that, although early remodeling of Kir/HCN function initiates membrane instability, later changes in additional conductances consolidate a hyperexcitable phenotype. In this respect, the time-dependent alterations in AP dynamics by phase–plane analysis provided further mechanistic insights into this temporal sequence, suggesting a progressive imbalance between Na^+ and K^+ conductances in *Epm2a*^{R240X} neurons. Indeed, the increased upstroke slope (maximal dV/dt) in *Epm2a*^{R240X} neurons compared to WT, points to a gain of function in NaV^+ conductances or accelerated activation kinetics, changes that lower AP threshold, thereby accelerating the onset of APs and enhancing excitability.[42–45] Moreover, the descending slope is affected only slightly in young (1- to 3-month-old) mice while is decreased in 12-month-old *Epm2a*^{R240X} mice. This deceleration of the descending phase is consistent with a loss or delayed activation of potassium currents, particularly delayed rectifier (Kv2, Kv3)[46] and possibly BK channels, which are essential for rapid repolarization.[47] This slowing of repolarization prolongs AP duration, increasing the time window for Ca^{2+} entry through voltage-gated calcium channels.[48] The resulting elevation in intracellular Ca^{2+} is expected to potentiate neurotransmitter release and synaptic plasticity mechanisms.[49]

Moreover, the ascending phase of the phase–plane plot at 12 months displayed a "shoulder" more evident in *Epm2a*^{R240X}, indicating a slowed but amplified depolarizing drive. This deflection is primarily attributable to the recruitment of voltage-gated Na^+ channels, whose increased availability results in a steeper slope during the rising phase.[42] However, the voltage window of the shoulder also matches the activation range of T-type Ca^{2+} channels,[50,51] suggesting that their contribution may further sustain depolarization. Such Ca^{2+} entry not only anticipates AP initiation but also provides a powerful signal for downstream plasticity-related pathways.[49] Moreover, in DG granule cells, changes in AP threshold have been associated with the expression of Kv7 channels at the axon initial segment, which in turn are modulated by calcium entry through T-type Ca^{2+} channels in the axon.[52] In *Epm2a*^{R240X} neurons, the shoulder is broader and more pronounced, consistent with a synergistic effect of increased Na^+ conductance and possible upregulation or disinhibition of low-threshold Ca^{2+} channels. This altered excitability profile is further reinforced by the reduced Ih-dependent rectification, which normally opposes excessive hyperpolarization and stabilizes the membrane potential.[53] A diminished Ih increases input resistance at hyperpolarized potentials, thereby amplifying the impact of depolarizing currents. Together, these alterations create a condition of increased excitability and a lower threshold for synaptic integration. The combination of a stronger Na^+/Ca^{2+}-dependent shoulder and reduced Ih may underlie the hyperplasticity observed in aged *Epm2a*^{R240X} mice. The enhanced depolarizing drive facilitates the induction of Hebbian forms of synaptic plasticity, whereas the greater Ca^{2+} influx through T-type channels provides a critical second messenger for long-term modifications of synaptic strength.[49,54] Thus, intrinsic excitability changes and synaptic plasticity reinforcement appear tightly

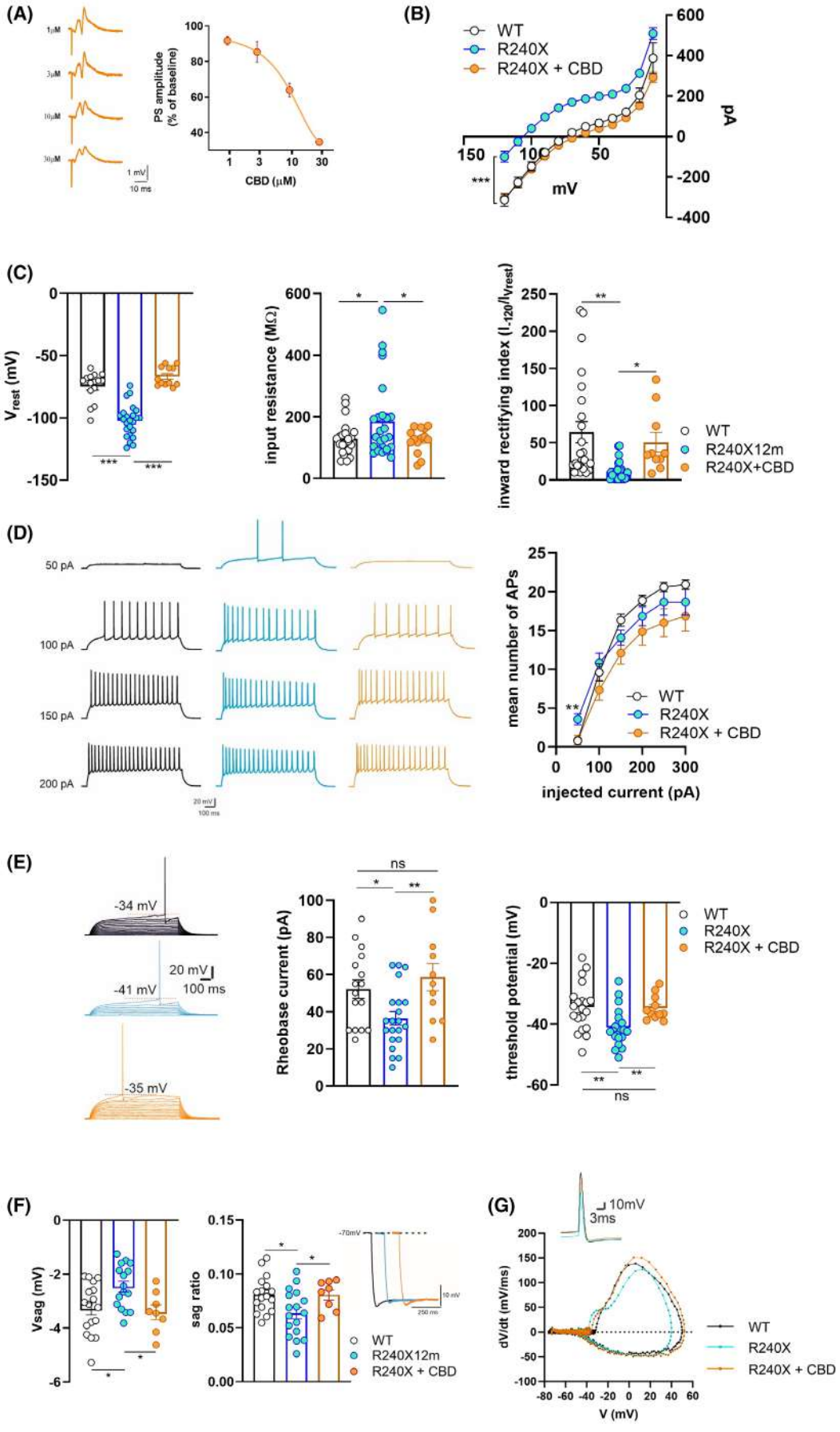

FIGURE 5 Effect of CBD on 12-month-old *Epm2a*^{R240X} mice DG granule cells excitability. (A) Effect of CBD on physiological synaptic transmission in the DG region. Left: Representative traces of PSs recorded on increasing doses of CBD. Dose–response curve showing that CBD 3 μM is not able to alter the physiological synaptic transmission (CBD 1 μM: 91.7 ± 2.5% of baseline; CBD 3 μM: 85.4 ± 5.9% of baseline; CBD 10 μM: 63.8 ± 3.8% of baseline; CBD 30 μM: 34.6 ± .7% of baseline; IC50: 10.96 ± .08 nM). (B) CBD 3 μM restores the physiological current–voltage relationship in the granule cells of 12-month-old *Epm2a*^{R240X} mice ($p < .0001$, $F_{(1,35)} = 126.2$, R240X vs R240X + CBD, two-way ANOVA). (C) Bar graphs showing that CBD normalizes the hyperpolarized resting membrane potential (left), the IR at hyperpolarized potentials (middle) and the IRI (right) to control levels (V_{rest}: WT = −74.5 ± 3 mV, $n = 15$; R240X = −102.5 ± 2.6 mV, $n = 24$, $p < .0001$ vs WT; R240X + CBD = −66.7 ± 2.2 mV, $n = 12$, $p < .0001$ vs R240X; IR: WT = 128.3 ± 11.18 MΩ, $n = 23$; R240X = 185.2 ± 24.9 MΩ, $n = 26$, $p = .045$ vs WT; R240X + CBD = 124.8 ± 10.9 MΩ, $n = 14$, $p = .033$ vs R240X; IRI: WT = 64.14 5 ± 14.2, $n = 24$; R240X = 11.66 ± 2.58, $n = 26$, $p = .013$ vs WT; R240X + CBD = 50.47 ± 13.3, $n = 10$, $p = .0174$ vs R240X; unpaired Student's *t* test with Welch's correction). (D) Patterns of AP firing of DG granule cells in WT (black) and *Epm2a*^{R240X} mice in the absence (cyan) and in the presence of 3 μM CBD (orange). Note that CBD is able to recover the firing pattern discharge elicited by the first step of depolarizing current in 12-month-old *Epm2a*^{R240X} mice (WT: .6 ± 1.4, $n = 15$; R240X: 3.6 ± .7, $n = 19$, $p = .0016$ vs WT; R240X + CBD: .9 ± .6, $n = 10$, $p = .011$ vs R240X; unpaired Student's *t* test with Welch's correction). (E) Representative current–clamp recordings (5 pA–stepped depolarizing current injections; 1 s), scaled to show AP threshold (red dotted line), in DG granule cells from WT (black) and *Epm2a*^{R240X} mice in the absence (cyan) and in the presence of 3 μM CBD (orange). Bar graphs showing that 3 μM CBD is able to normalize the rheobase current (WT: 52.2 ± 5 pA, $n = 16$; 12m-R240X: 36.5 ± 3.6 pA, $n = 21$, $p = .0135$ vs WT; R240X + CBD: 58.6 ± 7.3 pA; $n = 11$, $p = .0048$ vs R240X, $p = .46$ vs WT; unpaired Student's *t* test with Welch's correction) and the threshold potential (WT: −34.4 ± 1.7 mV, $n = 20$; R240X: −41.2 ± 1.3 mV, $n = 21$, $p = .0037$ vs WT; R240X + CBD: −34.7 ± 1.2 mV; $n = 11$, $p = .0036$ vs R240X, $p = .91$ vs WT; unpaired Student's *t* test with Welch's correction) to physiological levels in 12-month-old *Epm2a*^{R240X} mice. (F) Bar graphs and representative traces showing that CBD normalizes Vsag (left) and sag ratio (right) to control values (Vsag: WT = −3.28 ± .2 mV, $n = 17$; R240X: −2.46 ± .2 mV, $n = 17$, $p = .012$ vs WT; R240X + CBD: −3.41 ± .3 mV, $n = 8$, $p = .013$ vs R240X, $p = .72$ vs WT; sag ratio: WT: .08 ± .004, $n = 17$; R240X: .063 ± .005, $n = 17$, $p = .013$ vs WT; R240X + CBD: .08 ± .005, $n = 8$, $p = .027$ vs R240X, $p = .95$ vs WT; unpaired Student's *t* test with Welch's correction) (G) Representative phase–plane plots (dV/dt vs membrane potential) are shown for WT (black), 12 month old *Epm2a*^{R240X} (cyan), and *Epm2a*^{R240X} + CBD (orange) neurons. Insets illustrate representative single action potential waveforms recorded in current-clamp configuration under each condition (calibration: 10 mV, 3 ms). Data are reported as means ± SEM; circles in bar graphs represent individual cells. *$p < .05$, **$p < .01$, ***$p < .001$.

coupled in the *Epm2a*^{R240X} model, offering a mechanistic explanation for the age-dependent emergence of pathological plasticity. Similar enhanced synaptic plasticity has been described in several genetic neuropathologies[55,56] and is associated with cognitive impairment. We previously demonstrated that old *Epm2a*^{R240X} mice exhibit cognitive deficits and hyperplasticity as well as enhanced epileptic-like activity and lower epileptic threshold.[11] This study assessed epileptic-like activity and synaptic plasticity in young *Epm2a*^{R240X} mice to determine if these alterations are present early in LD. Although the epileptic threshold is preserved, epileptic-like activity is already increased in 1- and 3-month-old *Epm2a*^{R240X} mice, albeit less than in older animals, demonstrating a time-dependent progression. LTP analysis in 3-month-old mice showed a significant increase compared to WT but a decrease compared to 12-month-old *Epm2a*^{R240X} mice. Conversely, 1-month-old mice exhibited physiological LTP. This indicates that network overexcitability is an early event in LD progression, preceding LBs and synaptic damage, defining a potential therapeutic intervention window.

Of interest, although time-dependent Aβ deposition has been reported in laforin knockout mice,[13] we demonstrate for the first time Aβ deposits in the hippocampus of *Epm2a*^{R240X} mice. Although Aβ deposition may contribute to LD pathophysiology, further studies will be required to determine its specific role in LD progression and in the hyperexcitability phenotype. Clinical and preclinical studies highlight that Aβ deposition and aberrant neuronal and network excitability are closely intertwined in a vicious cycle leading to dysfunctional network activity and neurodegeneration.[15,16]

Although we did not detect changes in glutamatergic receptor subunits, recent evidence suggests that glycogen accumulation in GABAergic interneurons may critically contribute to the onset of hyperexcitability, later reinforced by glutamate homeostasis dysregulation involving astrocytes.[57,58] Moreover, the presence of Aβ42 aggregates selectively in hippocampal regions of laforin-deficient mice at advanced stages[13] supports the notion of age- and cell type–dependent vulnerability contributing to disease progression. These observations highlight the need for future studies directly addressing GABAergic interneurons and astrocytic involvement in this model.

Another possibility is that altered excitability is associated with aberrant neurogenesis in this LD model. It is well documented that adult neurogenesis declines with physiological aging in mammals. In rodents, neurogenesis significantly decreases with age in both the subventricular zone and the DG niches, with proliferation almost completely lost by 20–24 months.[59] In contrast, in our LD model, we observed a progressive age-related increase in progenitor cells across all hippocampal regions, with significantly higher numbers in 12-month-old *Epm2a*^{R240X}

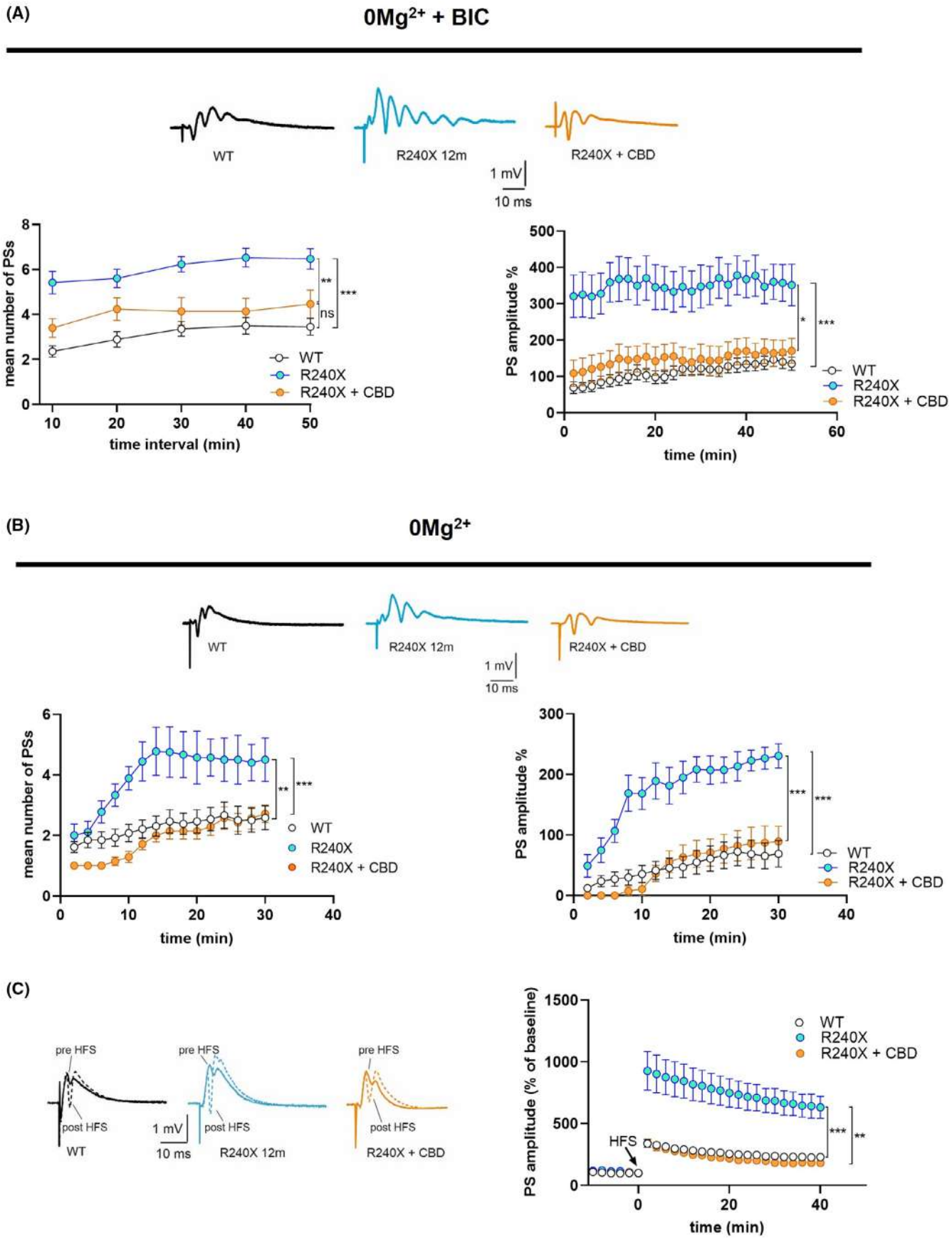

FIGURE 6 Effect of CBD on epileptic-like activity and LTP in the DG of 12-month-old *Epm2a*^{R240X} mice. (A) Representative traces and time-course graph of FPs recorded in magnesium-free +.1 μM bicuculline ACSF solution in the DG of WT (black traces) and 12-month-old *Epm2a*^{R240X} mice in the absence (cyan traces) or presence (orange traces) of 3 μM CBD. Note that 3 μM CBD is able to recover the mean number and amplitude of PSs in 12-month-old *Epm2a*^{R240X} mice to control levels (PS number: WT: 3.4 ± .4, $n = 20$; R240X: 6.5 ± .4, $n = 13$, $p < .0001$, $F_{(1,31)} = 52.54$ vs WT; R240X + CBD: 4.5 ± .6, $n = 6$, $p = .0036$, $F_{(1,17)} = 11.36$ vs R240X, $p = .09$ $F_{(1,24)} = 3.109$ vs WT; PS amplitude: WT: 135 ± 17.9%, $n = 26$; R240X: 351 ± 57.0%, $n = 13$, $p < .0001$, $F_{(1,37)}$=29.01 vs WT; R240X + CBD: 170 ± 34.3%, $n = 7$, $p = .017$, $F_{(1,18)} = 6.85$ vs R240X, $p = .34$, $F_{(1,31)} = .93$ vs WT; two-way ANOVA). (B) Representative traces and time-course graph of FPs recorded in magnesium-free ACSF solution in the DG of WT (black traces) and 12-month-old *Epm2a*^{R240X} mice in the absence (cyan traces) or in the presence (orange traces) of 3 μM CBD. Note that 3 μM CBD is able to recover the mean number and amplitude of PSs, in 12-month-old *Epm2a*^{R240X} mice to control levels (*PS number*: WT: 2.6 ± .4, $n = 13$; R240X: 4.5 ± .72, $n = 10$, $p = .0012$, $F_{(1,19)} = 14.46$ vs WT; R240X + CBD: 2.7 ± .28, $n = 7$, $p < .0001$, $F_{(1,14)} = 35.43$ vs R240X, $p = .34$, $F_{(1,17)} = .97$ vs WT; *PS amplitude*: WT: 75.8 ± 22.9%, $n = 14$; R240X: 240 ± 20.3%, $n = 11$, $p < .0001$, $F_{(1,24)} = 27.83$ vs WT; R240X + CBD: 89.2 ± 25.3%, $n = 7$, $p = .0002$, $F_{(1,17)} = 22.56$ vs R240X, $p = .81$, $F_{(1,19)} = .057$ vs WT; two-way ANOVA). (C) Representative traces and time-course graph of PSs recorded before (continuous line) and 40 min after (dotted line) the HFS protocol in WT (black), 12-month-old *Epm2a*^{R240X} (cyan). and in *Epm2a*^{R240X} mice in the presence of 3 μM CBD (orange). Note that treatment with 3 μM CBD is able to restore the aberrant LTP observed in the DG of *Epm2a*^{R240X} to physiological levels (WT: 230 ± 26.4%, $n = 13$; R240X: 632 ± 89.3%, $n = 10$, $p = .0001$, $F_{(1,20)}$=22.74 vs WT; R240X + CBD: 182 ± 15.4%, $n = 7$, $p = .0019$, $F_{(1,14)} = 14.6$ vs R240X, $p = .4$, $F_{(1,18)}$=.72 vs WT; two-way ANOVA). Data are reported as means ± SEM, *n* refers to the number of slices.

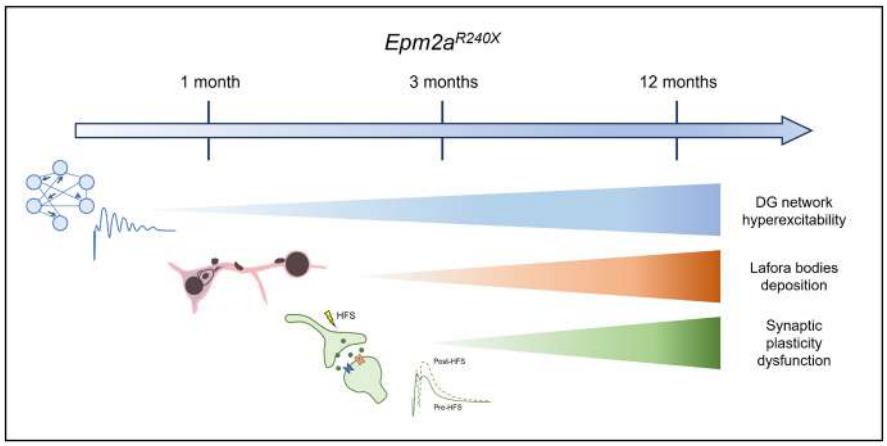

FIGURE 7 Network hyperexcitability as an early event in LD progression. Our results suggest that network hyperexcitability might represent one of the early pathogenic steps in LD, preceding synaptic deterioration and clear LBs or Aβ deposition. The schematic representation of LBs was made taking inspiration from the original drawing of LBs made by Lafora.[32]

mice compared to WT mice. This suggests that aberrant neurogenesis could be a pathological response to hyperexcitability rather than baseline neurogenesis. Similar increases in nestin-positive cells have been described in multiple studies of epilepsy, including the temporal neocortex of patients with intractable epilepsy,[60] the hippocampal region of patients with temporal lobe epilepsy,[61] and the hippocampus of rats following status epilepticus.[62] A complex interplay between hyperexcitability and aberrant neurogenesis has been proposed, where seizures stimulate hippocampal neurogenesis, leading to an overactive state due to the abnormal integration of new neurons. These newly generated neurons may enhance network excitability, creating a vicious cycle of hyperexcitability and aberrant neurogenesis.[63–65] Moreover, recent work has suggested that immature neurons and astrocytes, generated through aberrant neurogenesis and astrogenesis in mesial temporal lobe epilepsy may further contribute to epileptogenesis.[66] To investigate our hypothesis that hLTP results from enhanced excitability, we reduced excitability in the hippocampal slices of 12-month-old *Epm2a*^{R240X} mice using CBD, an emerging anti-seizure drug. CBD has recently been proposed as a viable therapeutic substitute for refractory seizure disorders like Lennox–Gastaut syndrome and Dravet syndrome (DS).[22] Compared with traditional anti-seizure drugs, CBD is an effective anticonvulsant with fewer neurotoxic effects[67] and does not induce excitability in the CNS, thereby reducing both the duration and amplitude of the post-discharge cAMP response element-binding protein (CREB).[68] CBD has been tested in several epilepsy animal models,[69–71] consistently showing anti-seizure effects.

More than 50 molecular targets have been identified for CBD,[67,72,73] many of which are ionotropic and metabotropic receptors involved in neuronal function, synaptic calcium mobilization, and membrane potential. CBD could indeed exert a functional antagonism of orphan G protein–coupled receptor-55 (GPR55),[74] known to be involved in the mobilization of cellular Ca^{2+} stores, and influence neuronal depolarization by activating and

rapidly desensitizing transient receptor potential vanilloid-1 (TRPV1) receptors.[75,76] Other studies showed that CBD might act as positive allosteric modulator of $GABA_A$ receptor[77] and as negative modulator of cation-permeable homomeric α7 nicotinic acetylcholine receptors (α7-nAChR),[78–80] and both effects reduce seizure susceptibility. Finally, the CBD-dependent modulation of neuronal membrane potential and excitability, counteracting epileptogenesis, is further supported by reports showing that this drug can inhibit voltage-gated sodium channel (Nav), hypothetically by stabilizing its inactivated channel states[81,82] and, potentially, T-type voltage-gated calcium channels (VGCCs).[83] As expected, treating DG slices with CBD, at a concentration that does not alter physiological transmission, reduced epileptic-like activity and restored the epileptic threshold to control levels in 12-month-old *Epm2a*^{R240X} mice. The mechanisms through which CBD modulates DG excitability in *Epm2a*^{R240X} mice still need to be elucidated, but may involve CBD's multi-target action. In line with this broad pharmacological profile, our findings indicate that CBD counteracts the age-dependent alterations in both subthreshold currents and suprathreshold channel dynamics in *Epm2a*^{R240X} neurons, thereby contributing to the normalization of excitability, but future studies should characterize which molecular pathways are implicated. Hopefully, such studies might unveil novel therapeutic targets for LD, beyond known metabolic effects induced by genetic abnormalities linked to this disease.

It is intriguing that CBD treatment rescued LTP in the DG of *Epm2a*^{R240X} mice to control levels. This is the first demonstration that reducing excitability can constitute a strategy to rescue synaptic plasticity in a mouse model of LD. This beneficial effect on synaptic plasticity could hypothetically lead to an amelioration of cognitive deficits characterizing LD, which should be tested in future studies. Of note, previous reports showed that CBD's anti-seizure effects are paralleled by improvements in cognitive and behavioral deficits in the *Scn1a*$^{+/-}$ genetic mouse model of DS.[71,84]

Our results shed light on neuronal alterations in the early LD stages and provide proof of principle that modulating neuronal excitability can rescue synaptic dysfunction in this LD model.

ACKNOWLEDGMENTS

We thank Prof. Paolo Calabresi for critically revising the manuscript, Chiara Galizia for her technical support in biochemical experiments, Francisco Wandosell for his generous gift of 4G8 and nestin antibodies. We also thank the Animal Facility of Instituto de Investigación Sanitaria-Fundación Jiménez Díaz for their technical assistance, and the "DEFEAT-LD study group" of PNRR-MR1-2022-12376430 - Project 'Drug discovEry and repurposing to Find a trEAtmenT for Lafora Disease (DEFEAT-LD)'. Open access publishing facilitated by Universita degli Studi di Perugia, as part of the Wiley - CRUI-CARE agreement.

FUNDING INFORMATION

This work was supported by grants from the Fondazione Malattie Rare Mauro Baschirotto BIRD Onlus to M.P.S., C.C., M.S., and L.Z.P; from the Associazione Stella Costa di Amalfi to C.C.; from PNRR-MR1-2022-12376430 - Project "Drug discovEry and repurposing to Find a trEAtmenT for Lafora Disease (DEFEAT-LD)" – to C.C.; from the Spanish Ministry of Economy [Rti2018-095784b-100SAF MCI/AEI/FEDER, UE] to J.M.S. and M.P.S.; from the Tatiana Pérez de Guzmán el Bueno Foundation to M.P.S. and J.M.S.; from the Centro de Investigación Biomédica en Red de Enfermedades Raras (CIBERER) [ACCI 2020, 23 - U744] to M.P.S.; from the AEVEL Foundation to J.M.S. and L.Z.P.; and from the National Institute of Neurological Disorders and Stroke of the National Institutes of Health [P01NS097197], which established the Lafora Epilepsy Cure Initiative (LECI), to J.M.S. and M.P.S. LB is supported by a research fellowship FISM - Fondazione Italiana Sclerosi Multipla - cod. 2023/BR/005 and financed or co-financed with the "5 per mille" public funding. A.T. is supported by the Italian Ministry of University and Research PRIN 2022, grant 2022CAKAHL and PRIN 2022 Next Generation EU-PNRR-M4C2, grant P2022374Y9.

CONFLICT OF INTEREST STATEMENT

Cinzia Costa has received research funding, speaker honoraria, and travel support from Bial, Eisai, Europe Limited, GW Pharma, Jazz Pharmaceuticals, Lusopharma, PIAM Pharma, and UCB Pharma. None of these companies had any role in the study design, data collection, analysis or interpretation, manuscript preparation, or the decision to submit the article for publication. None of the other authors have any interests to disclose. We confirm that we have read the Journal's position on issues involved in ethical publication and affirm that this report is consistent with those guidelines.

DATA AVAILABILITY STATEMENT

The data that support the findings of this study are available on request from the corresponding author. The data are not publicly available due to privacy or ethical restrictions.

ORCID

Cinzia Costa https://orcid.org/0000-0002-4862-4221
Anna Aurora Taddei https://orcid.org/0009-0002-6731-2343

Luis Zafra-Puerta https://orcid.org/0000-0002-1807-7538
Miriam Sciaccaluga https://orcid.org/0000-0001-7951-8045

REFERENCES

1. Monaghan TS, Delanty N. Lafora disease: epidemiology, pathophysiology and management. CNS Drugs. 2010;24(7):549–61.
2. Serratosa JM, Delgado-Escueta AV, Posada I, Shih S, Drury I, Berciano J, et al. The gene for progressive myoclonus epilepsy of the Lafora type maps to chromosome 6q. Hum Mol Genet. 1995;4(9):1657–63.
3. Serratosa JM, Gómez-Garre P, Gallardo ME, Anta B, de Bernabé DB, Lindhout D, et al. A novel protein tyrosine phosphatase gene is mutated in progressive myoclonus epilepsy of the Lafora type (EPM2). Hum Mol Genet. 1999;8(2):345–52.
4. Minassian BA, Lee JR, Herbrick JA, Huizenga J, Soder S, Mungall AJ, et al. Mutations in a gene encoding a novel protein tyrosine phosphatase cause progressive myoclonus epilepsy. Nat Genet. 1998;20(2):171–4.
5. Chan EM, Young EJ, Ianzano L, Munteanu I, Zhao X, Christopoulos CC, et al. Mutations in NHLRC1 cause progressive myoclonus epilepsy. Nat Genet. 2003;35(2):125–7.
6. Nitschke F, Ahonen SJ, Nitschke S, Mitra S, Minassian BA. Lafora disease - from pathogenesis to treatment strategies. Nat Rev Neurol. 2018;14(10):606–17.
7. García-Gimeno MA, Knecht E, Sanz P. Lafora disease: a ubiquitination-related pathology. Cells. 2018;7(8):87.
8. Ganesh S, Delgado-Escueta AV, Sakamoto T, Avila MR, Machado-Salas J, Hoshii Y, et al. Targeted disruption of the Epm2a gene causes formation of Lafora inclusion bodies, neurodegeneration, ataxia, myoclonus epilepsy and impaired behavioral response in mice. Hum Mol Genet. 2002;11(11):1251–62.
9. DePaoli-Roach AA, Tagliabracci VS, Segvich DM, Meyer CM, Irimia JM, Roach PJ. Genetic depletion of the malin E3 ubiquitin ligase in mice leads to lafora bodies and the accumulation of insoluble laforin. J Biol Chem. 2010;285(33):25372–81.
10. Turnbull J, DePaoli-Roach AA, Zhao X, Cortez MA, Pencea N, Tiberia E, et al. PTG depletion removes Lafora bodies and rescues the fatal epilepsy of Lafora disease. PLoS Genet. 2011;7(4):e1002037.
11. Burgos DF, Sciaccaluga M, Worby CA, Zafra-Puerta L, Iglesias-Cabeza N, Sánchez-Martín G, et al. Epm2a^{R240X} knock-in mice present earlier cognitive decline and more epileptic activity than Epm2a$^{-/-}$ mice. Neurobiol Dis. 2023;181:106119.
12. DiNuzzo M, Mangia S, Maraviglia B, Giove F. Does abnormal glycogen structure contribute to increased susceptibility to seizures in epilepsy? Metab Brain Dis. 2015;30(1):307–16.
13. Puri R, Suzuki T, Yamakawa K, Ganesh S. Dysfunctions in endosomal-lysosomal and autophagy pathways underlie neuropathology in a mouse model for Lafora disease. Hum Mol Genet. 2012;21(1):175–84.
14. d'Orsi G, Farolfi A, Muccioli L, Palumbo O, Palumbo P, Modoni S, et al. Association of CSF and PET markers of neurodegeneration with electroclinical progression in Lafora disease. Front Neurol. 2023;14:1202971.
15. Romoli M, Sen A, Parnetti L, Calabresi P, Costa C. Amyloid-β: a potential link between epilepsy and cognitive decline. Nat Rev Neurol. 2021;17(8):469–85.
16. Sciaccaluga M, Megaro A, Bellomo G, Ruffolo G, Romoli M, Palma E, et al. An unbalanced synaptic transmission: cause or consequence of the amyloid oligomers neurotoxicity? Int J Mol Sci. 2021;22(11):5991.
17. Giorgio J, Adams JN, Maass A, Jagust WJ, Breakspear M. Amyloid induced hyperexcitability in default mode network drives medial temporal hyperactivity and early tau accumulation. Neuron. 2024;112(4):676–86.e4.
18. Kamondi A, Grigg-Damberger M, Löscher W, Tanila H, Horvath AA. Epilepsy and epileptiform activity in late-onset Alzheimer disease: clinical and pathophysiological advances, gaps and conundrums. Nat Rev Neurol. 2024;20(3):162–82.
19. Taneja K, Ganesh S. Dendritic spine abnormalities correlate with behavioral and cognitive deficits in mouse models of Lafora disease. J Comp Neurol. 2021;529(6):1099–120.
20. Zafra-Puerta L, Iglesias-Cabeza N, Burgos DF, Sciaccaluga M, González-Fernández J, Bellingacci L, et al. Gene therapy for Lafora disease in the *Epm2a*−/− mouse model. Mol Ther. 2024;32(7):2130–49.
21. Cifelli P, Ruffolo G, De Felice E, Alfano V, van Vliet EA, Aronica E, et al. Phytocannabinoids in neurological diseases: could they restore a physiological GABAergic transmission? Int J Mol Sci. 2020;21(3):723.
22. Sciaccaluga M, Ruffolo G, Palma E, Costa C. Traditional and innovative anti-seizure medications targeting key Physiopathological mechanisms: focus on neurodevelopment and neurodegeneration. Curr Neuropharmacol. 2023;21(8):1736–54.
23. Devinsky O, Cross JH, Laux L, Marsh E, Miller I, Nabbout R, et al. Trial of Cannabidiol for drug-resistant seizures in the Dravet syndrome. N Engl J Med. 2017;376(21):2011–20.
24. Patel AD, Mazurkiewicz-Bełdzińska M, Chin RF, Gil-Nagel A, Gunning B, Halford JJ, et al. Long-term safety and efficacy of add-on cannabidiol in patients with Lennox-Gastaut syndrome: results of a long-term open-label extension trial. Epilepsia. 2021;62(9):2228–39.
25. Man H-Y, Sekine-Aizawa Y, Huganir RL. Regulation of {alpha}-amino-3-hydroxy-5-methyl-4-isoxazolepropionic acid receptor trafficking through PKA phosphorylation of the Glu receptor 1 subunit. Proc Natl Acad Sci USA. 2007;104(9):3579–84.
26. Christian KM, Song H, Ming G. Functions and dysfunctions of adult hippocampal neurogenesis. Annu Rev Neurosci. 2014;37:243–62.
27. von Bohlen und Halbach O. Immunohistological markers for proliferative events, gliogenesis, and neurogenesis within the adult hippocampus. Cell Tissue Res. 2011;345(1):1–19.
28. Jiang N, Cupolillo D, Grosjean N, Muller E, Deforges S, Mulle C, et al. Impaired plasticity of intrinsic excitability in the dentate gyrus alters spike transfer in a mouse model of Alzheimer's disease. Neurobiol Dis. 2021;154:105345.
29. Smith LA, Goodman AM, McMahon LL. Dentate granule cells are Hyperexcitable in the TgF344-AD rat model of Alzheimer's disease. Front Synaptic Neurosci. 2022;14:826601.
30. Burgos DF, Cussó L, Sánchez-Elexpuru G, Calle D, Perpinyà MB, Desco M, et al. Structural and functional brain abnormalities in mouse models of Lafora disease. Int J Mol Sci. 2020;21(20):7771.
31. Valles-Ortega J, Duran J, Garcia-Rocha M, Bosch C, Saez I, Pujadas L, et al. Neurodegeneration and functional impairments associated with glycogen synthase accumulation in a mouse model of Lafora disease. EMBO Mol Med. 2011;3(11):667–81.

32. Lafora GR, Glueck B. Beitrag zur Histopathologie der myoklonischen Epilepsie. Z Für Gesamte Neurol Psychiatr. 1911;6(1):1–14.
33. Smith LA, McMahon LL. Deficits in synaptic function occur at medial perforant path-dentate granule cell synapses prior to Schaffer collateral-CA1 pyramidal cell synapses in the novel TgF344-Alzheimer's disease rat model. Neurobiol Dis. 2018;110:166–79.
34. Berg RW, Ditlevsen S. Synaptic inhibition and excitation estimated via the time constant of membrane potential fluctuations. J Neurophysiol. 2013;110(4):1021–34.
35. Maccaferri G, Mangoni M, Lazzari A, DiFrancesco D. Properties of the hyperpolarization-activated current in rat hippocampal CA1 pyramidal cells. J Neurophysiol. 1993;69(6):2129–36.
36. Surges R, Freiman TM, Feuerstein TJ. Input resistance is voltage dependent due to activation of Ih channels in rat CA1 pyramidal cells. J Neurosci Res. 2004;76(4):475–80.
37. He C, Chen F, Li B, Hu Z. Neurophysiology of HCN channels: from cellular functions to multiple regulations. Prog Neurobiol. 2014;112:1–23.
38. Lupica CR, Bell JA, Hoffman AF, Watson PL. Contribution of the hyperpolarization-activated current (I(h)) to membrane potential and GABA release in hippocampal interneurons. J Neurophysiol. 2001;86(1):261–8.
39. Stegen M, Kirchheim F, Hanuschkin A, Staszewski O, Veh RW, Wolfart J. Adaptive intrinsic plasticity in human dentate gyrus granule cells during temporal lobe epilepsy. Cereb Cortex. 2012;22(9):2087–101.
40. Mishra P, Narayanan R. Heterogeneities in intrinsic excitability and frequency-dependent response properties of granule cells across the blades of the rat dentate gyrus. J Neurophysiol. 2020;123(2):755–72.
41. Nolan MF, Dudman JT, Dodson PD, Santoro B. HCN1 channels control resting and active integrative properties of stellate cells from layer II of the entorhinal cortex. J Neurosci. 2007;27(46):12440–51.
42. Bean BP. The action potential in mammalian central neurons. Nat Rev Neurosci. 2007;8(6):451–65.
43. Kole MHP, Ilschner SU, Kampa BM, Williams SR, Ruben PC, Stuart GJ. Action potential generation requires a high sodium channel density in the axon initial segment. Nat Neurosci. 2008;11(2):178–86.
44. Catterall WA. Sodium channels, inherited epilepsy, and antiepileptic drugs. Annu Rev Pharmacol Toxicol. 2014;54:317–38.
45. Kole MHP, Stuart GJ. Signal processing in the axon initial segment. Neuron. 2012;73(2):235–47.
46. Rudy B, McBain CJ. Kv3 channels: voltage-gated K+ channels designed for high-frequency repetitive firing. Trends Neurosci. 2001;24(9):517–26.
47. Johnston D, Christie BR, Frick A, Gray R, Hoffman DA, Schexnayder LK, et al. Active dendrites, potassium channels and synaptic plasticity. Philos Trans R Soc B Biol Sci. 2003;358(1432):667–74.
48. Debanne D, Campanac E, Bialowas A, Carlier E, Alcaraz G. Axon physiology. Physiol Rev. 2011;91(2):555–602.
49. Magee JC, Johnston D. A synaptically controlled, associative signal for Hebbian plasticity in hippocampal neurons. Science. 1997;275(5297):209–13.
50. Huguenard JR. Low-threshold calcium currents in central nervous system neurons. Annu Rev Physiol. 1996;58:329–48.
51. Perez-Reyes E. Molecular physiology of low-voltage-activated t-type calcium channels. Physiol Rev. 2003;83(1):117–61.
52. Martinello K, Huang Z, Lujan R, Tran B, Watanabe M, Cooper EC, et al. Cholinergic afferent stimulation induces axonal function plasticity in adult hippocampal granule cells. Neuron. 2015;85(2):346–63.
53. Magee JC. Dendritic hyperpolarization-activated currents modify the integrative properties of hippocampal CA1 pyramidal neurons. J Neurosci. 1998;18(19):7613–24.
54. Johnston D, Narayanan R. Active dendrites: colorful wings of the mysterious butterflies. Trends Neurosci. 2008;31(6):309–16.
55. Wilson JF, Lodhia V, Courtney DP, Kirk IJ, Hamm JP. Evidence of hyper-plasticity in adults with autism spectrum disorder. Res Autism Spectr Disord. 2017;43–44:40–52.
56. Iure A, Mazzocchetti P, Bastioli G, Picconi B, Costa C, Marchionni I, et al. Differential effect of FHM2 mutation on synaptic plasticity in distinct hippocampal regions. Cephalalgia. 2019;39(10):1333–8.
57. Muñoz-Ballester C, Santana N, Perez-Jimenez E, Viana R, Artigas F, Sanz P. In vivo glutamate clearance defects in a mouse model of Lafora disease. Exp Neurol. 2019;320:112959.
58. Ortolano S, Vieitez I, Agis-Balboa RC, Spuch C. Loss of GABAergic cortical neurons underlies the neuropathology of Lafora disease. Mol Brain. 2014;7:7.
59. Babcock KR, Page JS, Fallon JR, Webb AE. Adult hippocampal neurogenesis in aging and Alzheimer's disease. Stem Cell Rep. 2021;16(4):681–93.
60. Wang L, Wang X, Yuan J, Xi Z, Xue T, Li Y, et al. Nestin in the temporal neocortex of the intractable epilepsy patients. Neurochem Res. 2009;34(3):574–80.
61. Liu J, Reeves C, Jacques T, McEvoy A, Miserocchi A, Thompson P, et al. Nestin-expressing cell types in the temporal lobe and hippocampus: morphology, differentiation, and proliferative capacity. Glia. 2018;66(1):62–77.
62. Scorza CA, Arida RM, Cavalheiro EA, Naffah-Mazzacoratti MG, Scorza FA. Expression of nestin in the hippocampal formation of rats submitted to the pilocarpine model of epilepsy. Neurosci Res. 2005;51(3):285–91.
63. Cho K-O, Lybrand ZR, Ito N, Brulet R, Tafacory F, Zhang L, et al. Aberrant hippocampal neurogenesis contributes to epilepsy and associated cognitive decline. Nat Commun. 2015;6:6606.
64. Chen L, Xu Y, Cheng H, Li Z, Lai N, Li M, et al. Adult-born neurons in critical period maintain hippocampal seizures via local aberrant excitatory circuits. Signal Transduct Target Ther. 2023;8(1):225.
65. Lybrand ZR, Goswami S, Zhu J, Jarzabek V, Merlock N, Aktar M, et al. A critical period of neuronal activity results in aberrant neurogenesis rewiring hippocampal circuitry in a mouse model of epilepsy. Nat Commun. 2021;12(1):1423.
66. Ammothumkandy A, Ravina K, Wolseley V, Tartt AN, Yu P-N, Corona L, et al. Altered adult neurogenesis and gliogenesis in patients with mesial temporal lobe epilepsy. Nat Neurosci. 2022;25(4):493–503.
67. Dell'Isola GB, Verrotti A, Sciaccaluga M, Dini G, Ferrara P, Parnetti L, et al. Cannabidiol: metabolism and clinical efficacy in epileptic patients. Expert Opin Drug Metab Toxicol. 2024;20(3):119–31.
68. Patil N, Patil K, Jain M, Mohammed A, Yadav A, Dhanda PS, et al. A systematic study of molecular targets of cannabidiol in Alzheimer's disease. J Alzheimers Dis Rep. 2024;8(1):1339–60.

69. Jones NA, Hill AJ, Smith I, Bevan SA, Williams CM, Whalley BJ, et al. Cannabidiol displays antiepileptiform and antiseizure properties in vitro and in vivo. J Pharmacol Exp Ther. 2010;332(2):569–77.
70. Hill TDM, Cascio M-G, Romano B, Duncan M, Pertwee RG, Williams CM, et al. Cannabidivarin-rich cannabis extracts are anticonvulsant in mouse and rat via a CB1 receptor-independent mechanism. Br J Pharmacol. 2013;170(3):679–92.
71. Patra PH, Barker-Haliski M, White HS, Whalley BJ, Glyn S, Sandhu H, et al. Cannabidiol reduces seizures and associated behavioral comorbidities in a range of animal seizure and epilepsy models. Epilepsia. 2019;60(2):303–14.
72. Castillo-Arellano J, Canseco-Alba A, Cutler SJ, León F. The polypharmacological effects of cannabidiol. Molecules. 2023;28(7):3271.
73. Devinsky O, Cilio MR, Cross H, Fernandez-Ruiz J, French J, Hill C, et al. Cannabidiol: pharmacology and potential therapeutic role in epilepsy and other neuropsychiatric disorders. Epilepsia. 2014;55(6):791–802.
74. Rosenberg EC, Chamberland S, Bazelot M, Nebet ER, Wang X, McKenzie S, et al. Cannabidiol modulates excitatory-inhibitory ratio to counter hippocampal hyperactivity. Neuron. 2023;111(8):1282–300.e8.
75. Gray RA, Stott CG, Jones NA, Di Marzo V, Whalley BJ. Anticonvulsive properties of Cannabidiol in a model of generalized seizure are transient receptor potential vanilloid 1 dependent. Cannabis Cannabinoid Res. 2020;5(2):145–9.
76. Iannotti FA, Hill CL, Leo A, Alhusaini A, Soubrane C, Mazzarella E, et al. Nonpsychotropic plant cannabinoids, cannabidivarin (CBDV) and cannabidiol (CBD), activate and desensitize transient receptor potential vanilloid 1 (TRPV1) channels in vitro: potential for the treatment of neuronal hyperexcitability. ACS Chem Nerosci. 2014;5(11):1131–41.
77. Bakas T, van Nieuwenhuijzen PS, Devenish SO, McGregor IS, Arnold JC, Chebib M. The direct actions of cannabidiol and 2-arachidonoyl glycerol at GABAA receptors. Pharmacol Res. 2017;119:358–70.
78. Bertrand D, Lee C-HL, Flood D, Marger F, Donnelly-Roberts D. Therapeutic potential of α7 nicotinic acetylcholine receptors. Pharmacol Rev. 2015;67(4):1025–73.
79. Chrestia JF, Esandi MDC, Bouzat C. Cannabidiol as a modulator of α7 nicotinic receptors. Cell Mol Life Sci. 2022;79(11):564.
80. Mahgoub M, Keun-Hang SY, Sydorenko V, Ashoor A, Kabbani N, Al Kury L, et al. Effects of cannabidiol on the function of α7-nicotinic acetylcholine receptors. Eur J Pharmacol. 2013;720(1–3):310–9.
81. Ghovanloo M-R, Shuart NG, Mezeyova J, Dean RA, Ruben PC, Goodchild SJ. Inhibitory effects of cannabidiol on voltage-dependent sodium currents. J Biol Chem. 2018;293(43):16546–58.
82. Mason ER, Cummins TR. Differential inhibition of human Nav1.2 resurgent and persistent sodium currents by Cannabidiol and GS967. Int J Mol Sci. 2020;21(7):2454.
83. Ross HR, Napier I, Connor M. Inhibition of recombinant human T-type calcium channels by Delta9-tetrahydrocannabinol and cannabidiol. J Biol Chem. 2008;283(23):16124–34.
84. Kaplan JS, Stella N, Catterall WA, Westenbroek RE. Cannabidiol attenuates seizures and social deficits in a mouse model of Dravet syndrome. Proc Natl Acad Sci USA. 2017;114(42):11229–34.

SUPPORTING INFORMATION

Additional supporting information can be found online in the Supporting Information section at the end of this article.

How to cite this article: Costa C, Bellingacci L, Canonichesi J, Imperatore V, Taddei AA, Zafra-Puerta L, et al. Neuronal hyperexcitability: A key to unraveling hippocampal synaptic dysfunction in Lafora disease. Epilepsia. 2025;00:1–20. https://doi.org/10.1111/epi.70024